Neuron
Article

Two Rab2 Interactors Regulate Dense-Core Vesicle Maturation

Michael Ailion,[1,2,*] Mandy Hannemann,[3,4] Susan Dalton,[1] Andrea Pappas,[1] Shigeki Watanabe,[1] Jan Hegermann,[3,5,6] Qiang Liu,[1] Hsiao-Fen Han,[1] Mingyu Gu,[1] Morgan Q. Goulding,[2] Nikhil Sasidharan,[3] Kim Schuske,[1] Patrick Hullett,[1] Stefan Eimer,[3,5] and Erik M. Jorgensen[1,*]
[1]Howard Hughes Medical Institute, Department of Biology, University of Utah, Salt Lake City, UT 84112, USA
[2]Department of Biochemistry, University of Washington, Seattle WA, 98195, USA
[3]European Neuroscience Institute, 37077 Göttingen, Germany
[4]International Max Planck Research School Molecular Biology, 37077 Göttingen, Germany
[5]DFG research Center for Molecular Physiology of the Brain (CMPB), 37077 Göttingen, Germany
[6]Present address: Institute of Functional and Applied Anatomy, Medizinische Hochschule, D-30625 Hannover, Germany
*Correspondence: mailion@uw.edu (M.A.), jorgensen@biology.utah.edu (E.M.J.)
http://dx.doi.org/10.1016/j.neuron.2014.02.017

SUMMARY

Peptide neuromodulators are released from a unique organelle: the dense-core vesicle. Dense-core vesicles are generated at the *trans*-Golgi and then sort cargo during maturation before being secreted. To identify proteins that act in this pathway, we performed a genetic screen in *Caenorhabditis elegans* for mutants defective in dense-core vesicle function. We identified two conserved Rab2-binding proteins: RUND-1, a RUN domain protein, and CCCP-1, a coiled-coil protein. RUND-1 and CCCP-1 colocalize with RAB-2 at the Golgi, and *rab-2*, *rund-1*, and *cccp-1* mutants have similar defects in sorting soluble and transmembrane dense-core vesicle cargos. RUND-1 also interacts with the Rab2 GAP protein TBC-8 and the BAR domain protein RIC-19, a RAB-2 effector. In summary, a pathway of conserved proteins controls the maturation of dense-core vesicles at the *trans*-Golgi network.

INTRODUCTION

The nervous system has two modes of chemical signaling at synapses. Fast signaling occurs by the release of small-molecule neurotransmitters that activate ligand-gated ion channels. Slow signaling occurs by the release of neuromodulators, such as neuropeptides or monoamines, that activate G protein-coupled receptors. Fast neurotransmitters are released from synaptic vesicles, whereas many neuromodulators are released from dense-core vesicles (DCVs). A wide variety of biological processes are regulated by DCV secretion, including cell survival, neuronal development, synaptic plasticity, and excitability.

The pathway for the generation of DCVs in neurons is likely to be related to the generation of secretory vesicles in neuroendocrine cells such as chromaffin cells or the insulin-secreting cells of the pancreas (Borgonovo et al., 2006; Kim et al., 2006; Park and Loh, 2008; Tooze et al., 2001). The secretory granules are generated at the *trans*-Golgi and undergo several maturation steps, including the homotypic fusion of immature secretory granules, and removal of some soluble and transmembrane cargo (Ahras et al., 2006; Dittie et al., 1996; Kakhlon et al., 2006; Klumperman et al., 1998; Tooze et al., 1991; Urbé et al., 1998; Wendler et al., 2001). Cargo sorting relies on poorly defined motifs that probably interact with multiple sorting receptors (Dikeakos and Reudelhuber, 2007; Dikeakos et al., 2009). It is likely that DCVs in neurons undergo similar maturation processes at the Golgi, but some mechanisms may differ since these cells have a very different architecture.

The rich variety of small Rab GTPase proteins provides vesicles in all trafficking pathways with identity. Rabs orchestrate numerous aspects of vesicle trafficking including vesicle budding, transport, tethering, uncoating, and fusion (Stenmark, 2009; Zerial and McBride, 2001). There are about 60 different Rabs in humans and 26 in *C. elegans* (Lundquist, 2006; Pereira-Leal and Seabra, 2001). Rabs are localized to different intracellular compartments and help provide specificity to vesicular trafficking (Chavrier et al., 1990). In *C. elegans*, Rab2 (RAB-2) localizes to the Golgi (Sumakovic et al., 2009) and *rab-2* mutants (also known as *unc-108*) have defects in sorting soluble and transmembrane DCV cargos (Edwards et al., 2009; Sumakovic et al., 2009). Thus, there are likely to be Rab2 effectors involved in DCV cargo sorting.

Here we use a genetic screen to identify proteins involved in DCV function. We identify two proteins that are Rab2 interactors: RUND-1 and CCCP-1. RUND-1 and CCCP-1 are conserved proteins that colocalize with RAB-2 at the *trans*-Golgi. RUND-1 and CCCP-1 bind to activated RAB-2, and like *rab-2* mutants, *rund-1* and *cccp-1* mutants exhibit defects in sorting soluble and transmembrane DCV cargo. We conclude that RUND-1 and CCCP-1 may function as RAB-2 effectors in DCV maturation at the *trans*-Golgi.

RESULTS

A Genetic Screen for Regulators of Dense-Core Vesicle Function

In *C. elegans*, loss-of-function mutants in the trimeric G protein Gαq (encoded by *egl-30*) have a straight posture and are almost immobile on food (Brundage et al., 1996). Activated Gαq mutants

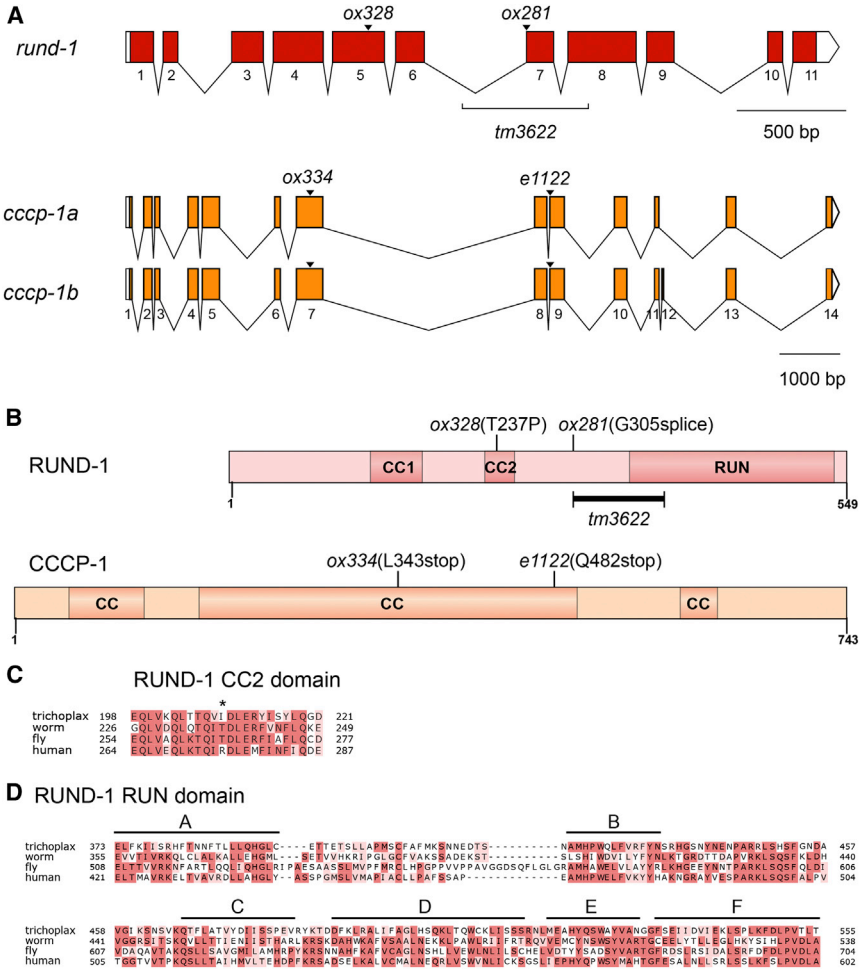

Figure 1. *rund-1* and *cccp-1* Encode Conserved Proteins

(A) Gene structures of *rund-1* and *cccp-1*. Colored boxes show coding segments. White boxes show UTRs. *cccp-1* has two transcripts.

(B) Domain structures of RUND-1 and CCCP-1. RUND-1 is a 549 amino acid protein with two coiled-coil (CC) domains and a RUN domain. *ox328* is a missense mutation in the second coiled-coil domain. *ox281* is a splice site mutation. The *tm3622* deletion is marked, but because this deletion starts in an intron (A), its effect on the protein is unknown. CCCP-1b is a 743 amino acid protein with multiple coiled-coil (CC) domains. The *ox334* and *e1122* mutations lead to premature stop codons.

(C) Alignment of the second coiled-coil domain of RUND-1 and its orthologs from *Trichoplax adhaerens* (Trichoplax), *C. elegans* (worm), *Drosophila melanogaster* (fly), and *Homo sapiens* (human). The position of the *ox328* T237P mutation is shown by an asterisk.

(D) Alignment of the RUN domain of RUND-1. The six conserved blocks A–F of the RUN domain (Callebaut et al., 2001) are marked with black bars. The *tm3622* deletion removes the A block but ends before the beginning of the B block. See also Figures S1 and S2.

exhibit the opposite phenotype; these mutants are hyperactive and exhibit tightly coiled body bends (Bastiani et al., 2003). Mutants in the DCV secretion protein CAPS (encoded by the *unc-31* gene) have a straight posture and are almost immobile on food (Avery et al., 1993), similar to *egl-30(lf)* mutants. Mutations in CAPS suppress activated alleles of Gαq (Charlie et al., 2006), suggesting that these proteins act in a pathway. Thus, mutations in other genes involved in DCV biogenesis and secretion should also suppress activated alleles of *egl-30*. We screened for genetic suppressors of the activating Gq mutation *egl-30(tg26)* (Doi and Iwasaki, 2002). *egl-30(tg26)* mutants have hyperactive, loopy locomotion and are smaller and slower growing than the wild-type (Movies S1 and S2 available online). We searched for less hyperactive animals among the F2 progeny of ENU-mutagenized *egl-30(tg26)*. We isolated six independent alleles of *unc-31*, validating the strategy of the screen. In addition, we isolated recessive mutations in six complementation groups with locomotion phenotypes reminiscent of *unc-31*, though somewhat weaker. These mutants exhibit a novel locomotion phenotype, which we call "unmotivated." When separated from the activated Gq mutation, the unmotivated mutants have a fairly normal posture but exhibit little spontaneous movement on food (Movie S3). However, they are capable of coordinated locomotion when stimulated. Conditions that stimulate movement include starvation, harsh touch, and UV light (Movies S3 and S4). Thus, these genes appear to function in the regulation of movement rather than the execution of coordinated movements.

We mapped and characterized in detail two of the six strong unmotivated mutants, *rund-1* and *cccp-1*. Two mutations (*ox281* and *ox328*) define the gene *rund-1*. Mutations at a second locus, conserved coiled-coil protein-1 (*cccp-1*), caused a similar phenotype. The mutation *cccp-1(ox334)* was isolated in the screen, and we found that it failed to complement an existing locomotion mutant *e1122* (previously known as *unc-81*).

rund-1 and *cccp-1* Encode Conserved Proteins

We cloned *rund-1* and *cccp-1* by standard methods (Experimental Procedures). The *rund-1* phenotype is fully rescued by the single gene T19D7.4. This open reading frame encodes a protein of 549 amino acids that has two coiled-coil domains in its N-terminal half and a RUN domain (RPIP8, UNC-14, and NESCA) near the C terminus (Figures 1A and 1B). RUN domains have been found in several proteins that bind to activated small GTPases of the Rab and Rap families and have been proposed to be effectors of these small G proteins (Callebaut et al., 2001). The mutation *ox281* is a splice site mutation; *ox328* introduces a proline into the second coiled-coil domain. We subsequently obtained a deletion allele *tm3622* that deletes the entire A block of the RUN domain (Figures 1A–1D). RUND-1 has a single conserved ortholog in other metazoans, including

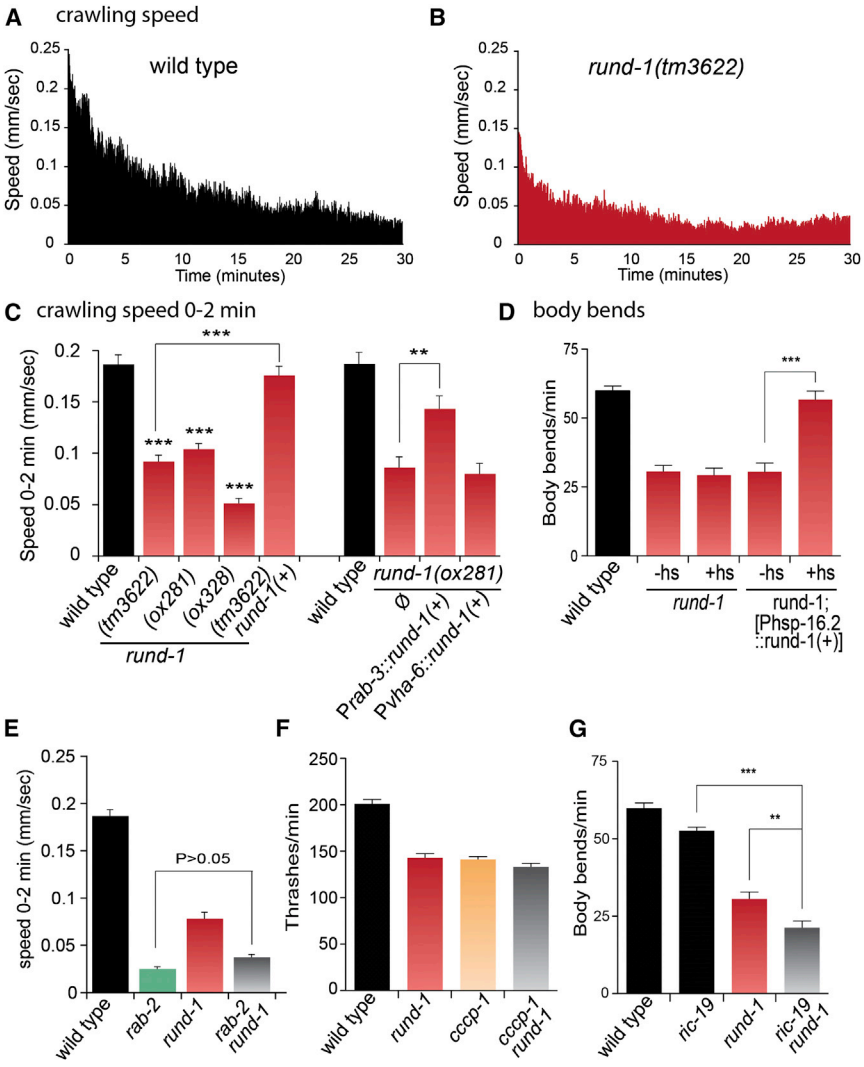

Figure 2. *rund-1* Mutants Exhibit Unmotivated Locomotion, but Respond to Stimulation

(A and B) Locomotion of wild-type (A) and *rund-1* mutants (B). The graphs plot mean speed during the 30 min after transfer to a new plate. Wild-type locomotion is stimulated by transfer and decays to baseline in 20 min. *rund-1* mutants are stimulated by transfer, but less than wild-type, and have a reduced baseline locomotion rate. n = 21–24 animals.

(C) Left: mean crawling speed during the first 2 min after transfer to a new plate. All three *rund-1* mutants exhibit reduced speed (***$p < 0.001$ versus wild-type) and the *rund-1(tm3622)* mutant is fully rescued by a *rund-1(+)* single-copy transgene. Right: expression of *rund-1(+)* in the nervous system rescues the *rund-1* mutant. The *rund-1* cDNA was expressed in either the nervous system (*Prab-3*) or the intestine (*Pvha-6*). Expression in the nervous system rescued (**$p < 0.01$), but expression in the intestine did not ($p > 0.05$). Error bars, SEM; n = 21–27 (left) and n = 9 (right).

(D) The *rund-1* locomotion defect is rescued by expression of a *rund-1(+)* transgene in mature animals. The frequency of body bends was measured during the first 2 min after transfer to a new plate. Heatshock-induced expression of *rund-1(+)* fully rescued the *rund-1* mutant defect (***$p < 0.001$ versus no heatshock). Heatshock did not affect *rund-1* ($p > 0.05$). +hs, heatshock; −hs, no heatshock. Error bars, SEM; n = 10.

(E) *rund-1* and *rab-2* act in the same genetic pathway to regulate locomotion. Mean speed was measured for 2 min after transfer to a new plate. The *rab-2 rund-1* double mutant is similar to the *rab-2* single mutant. Error bars, SEM; n = 24–31.

(F) *rund-1* and *cccp-1* act in the same genetic pathway to regulate locomotion. Frequency of body bends ("thrashes") in liquid was reduced for *rund-1(ox281)*, *cccp-1(ox334)* and *cccp-1(ox334); rund-1(ox281)* mutants compared to wild-type ($p < 0.001$). The *cccp-1 rund-1* double mutant is similar to the single mutants ($p > 0.05$). Error bars, SEM; n = 8–9.

(G) *rund-1* and *ric-19* act in parallel to regulate locomotion. Frequency of body bends was measured for two minutes after transfer to a new plate. *ric-19(pk690) rund-1(tm3622)* animals show a more severe defect than either single mutant (***$p < 0.001$; **$p < 0.01$). *ric-19* is not significantly different from wild-type ($p > 0.05$). The wild-type and *rund-1* data are identical to (D); these experiments were performed together. Error bars, SEM; n = 10.

See also Figures S3 and S7 and Table S2.

humans and *Drosophila*, and even the primitive metazoan *Trichoplax adhaerens* (Figure S1). RUND-1 shows conservation throughout the length of the protein; the second coiled-coil domain and the RUN domain are especially well conserved (Figures 1C and 1D).

RUND-1 and its human ortholog RUNDC1 are about 32% identical (Figure S1). We found that human RUNDC1 could rescue the worm *rund-1* mutants (Table S1; two-tailed $p < 0.0001$ for both strains, Fisher's exact test). RUNDC1 was tagged with tagRFP and exhibited a cellular localization pattern similar to the native RUND-1 (data not shown). Thus, the function and localization of RUND-1 are conserved in the human ortholog RUNDC1.

cccp-1 corresponds to the open reading frame Y49E10.23. *cccp-1* has two alternatively spliced transcripts, *cccp-1a* and *cccp-1b*, which encode proteins of 734 or 743 amino acids with multiple coiled-coil domains (Figures 1A and 1B). Like RUND-1, CCCP-1 has a single conserved ortholog in other metazoans including flies and humans and is not found outside metazoans (Figure S2). *cccp-1(ox334)* and *cccp-1(e1122)* both carry mutations leading to early stop codons.

rund-1 Mutants Exhibit Unmotivated Locomotion

The unmotivated phenotype is typified by inactivity on food (Movie S3). We used a computer-tracking system to characterize the movement of animals over a 30 min period. The speed of wild-type animals is highest immediately after a harsh mechanical stimulation and then decays over approximately the next 20 to 30 min to a stable baseline rate (Figure 2A). For *rund-1* mutants, the speed after stimulation is about half that of the

wild-type (Figures 2B and 2C; Figures S3B–S3D) and the animals become mostly inactive after 15 min; the phenotype is fully rescued by a single-copy insertion of the wild-type *rund-1(+)* gene (Figure 2C; Figure S3E).

The unmotivated phenotype is reminiscent of the locomotion of *unc-31*/CAPS mutants. CAPS is required for DCV fusion (Ann et al., 1997; Gracheva et al., 2007; Speese et al., 2007; Walent et al., 1992; Zhou et al., 2007) and may also regulate synaptic vesicle exocytosis (Gracheva et al., 2007; Jockusch et al., 2007). Mutants lacking CAPS/UNC-31 are paralyzed on food but not off food (Avery et al., 1993; Speese et al., 2007); *rund-1* mutants also exhibit increased speed off food. *rund-1* and *unc-31* mutants also have defects in egg laying and defecation and enter the dauer diapause stage at high temperature (Ailion et al., 1999; Avery et al., 1993; Speese et al., 2007; data not shown). Also, both *unc-31* and *rund-1* mutants can be suppressed by an activating mutation in the Gαs ortholog *gsa-1* (Charlie et al., 2006; data not shown). Thus, *rund-1* probably regulates a DCV pathway shared by CAPS.

Although the unmotivated phenotype resembles a worm behavior called ''quiescence,'' the resemblance is superficial (Van Buskirk and Sternberg, 2007; Gaglia and Kenyon, 2009; Singh et al., 2011; You et al., 2008). First, unlike *rund-1* mutants, quiescent animals do not forage for food or eat. Second, quiescence can be suppressed by mutations in the cyclic GMP-dependent protein kinase *egl-4*, but *rund-1* mutants are not suppressed by *egl-4* (data not shown). Third, quiescence depends on function of the ALA neuron and is suppressed by mutations that affect ALA development such as *ceh-17*. *rund-1* mutants, however, are not suppressed by *ceh-17* (data not shown). We conclude that unmotivated locomotion is a novel worm phenotype.

rund-1 Acts in Mature Neurons to Regulate Locomotion

We determined the cellular expression patterns of the *rund-1* and *cccp-1* genes by fusing their promoters to GFP. *Prund-1::GFP* was expressed in most or all neurons, the pharynx, the intestine, the spermatheca, and the uterus (Figures S4A and S4B) but was not seen in skin or muscle cells. *Pcccp-1::GFP* was also expressed in most or all neurons, the intestine, and the spermatheca but was not observed in the pharynx, skin, or muscle (Figure S4C).

To determine the cellular focus of the locomotory phenotype, we expressed *rund-1* and *cccp-1* under the control of tissue-specific promoters. Expression of *rund-1(+)* under the neuronal specific *rab-3* promoter rescued *rund-1* mutant locomotion, but expression of *rund-1* in the intestine using the *vha-6* promoter did not rescue (Figure 2C; Figures S3G–S3I). Under its own promoter, the tagged *cccp-1* cDNA rescued the *cccp-1* mutant locomotion defect (data not shown). This transgene was primarily expressed in the nervous system but at low levels. Interestingly, the *cccp-1* gene caused defects in locomotion in wild-type worms when expressed under the more highly expressed *rab-3* promoter (data not shown). Thus, both reduced expression and overexpression of *cccp-1* in neurons cause defects in locomotion.

To determine whether *rund-1* affects the development of neurons, we first examined neuronal architecture using the GABA neuron marker *Punc-47::GFP* (McIntire et al., 1997). No defects were seen in the *rund-1* mutant, indicating that *rund-1* is not generally required for axon guidance or maintenance (data not shown). Second, we examined the distribution of synaptic varicosities by imaging fluorescently tagged synaptobrevin, a synaptic vesicle protein (*Punc-129::mCherry::SNB-1*). No defects were observed in *rund-1* mutants, indicating that *rund-1* is not required for synapse development (Figures S5A and S5B).

The lack of a role in development was confirmed by rescuing the phenotype postdevelopmentally. We expressed the *rund-1* cDNA fused to tagRFP under a heat shock promoter. *rund-1* mutant animals carrying this construct were heat shocked at various stages of larval development. Twenty-four hours after heat-shock, adults were fully rescued for locomotion on food or in liquid (Figure 2D and data not shown). However, 5 hr after heat-shock, animals exhibited no discernible rescue, even though RFP expression was detected in neurons. Thus, *rund-1* acts in mature neurons but in a rather slow process.

RUND-1 and CCCP-1 Act in the Same Genetic Pathway as RAB-2

The presence of a RUN domain suggested that RUND-1 may interact with a small GTPase in either the Rab or Rap family. RAB-2 is a Golgi Rab that functions in DCV maturation in *C. elegans* (Edwards et al., 2009; Sumakovic et al., 2009). Mutants lacking the *rab-2* gene (also called *unc-108*) exhibit similar but somewhat stronger locomotion defects than *rund-1* (Chun et al., 2008; Edwards et al., 2009; Sumakovic et al., 2009). Like *rund-1*, *rab-2* mutants exhibit little spontaneous movement on food but move normally when stimulated by UV light (Edwards et al., 2009). Unlike *rund-1*, *rab-2* mutants cannot be stimulated by a harsh mechanical stimulus (Figure S7A).

The phenotypic similarity between *rund-1*, *cccp-1*, and *rab-2* mutants suggests that they may act in the same pathway, and analysis of double mutants supports this conclusion. First, *rab-2*, *rund-1*, and *cccp-1* mutations all suppress the hyperactive locomotion of the activated Gq mutant *egl-30(tg26)* (data not shown). Second, double mutants among *rab-2*, *rund-1*, and *cccp-1* do not show enhanced locomotion defects (Figures 2E and 2F; Figure S7A; data not shown). These data suggest that RAB-2, RUND-1, and CCCP-1 function together in DCV maturation.

DCV maturation involves the sorting of neuropeptide precursors into vesicles; the vesicles are then acidified, which activates the endopeptidases that cleave the precursors into mature neuropeptides. In *C. elegans*, there are four proprotein convertases that process neuropeptides. Most peptides in neurons are processed by the convertase EGL-3 (Husson et al., 2006; Kass et al., 2001), though other convertases can contribute to the processing of peptides and some peptides are not processed at all (Leinwand and Chalasani, 2013; Pierce et al., 2001). Interestingly, *egl-3* mutants have a weaker locomotion defect than the unmotivated mutants *rab-2*, *rund-1*, and *cccp-1*. However, when *egl-3* is combined with *rab-2*, *rund-1*, or *cccp-1*, the double mutants are essentially paralyzed (Figures S7B and S7C and data not shown), indicating that *egl-3* acts in parallel to these genes. The double mutants are both qualitatively and quantitatively similar to *unc-31*/CAPS mutants (Edwards et al., 2009;

A

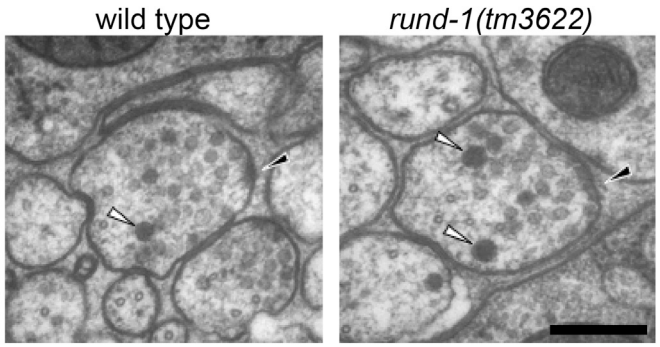

Figure 3. RUND-1 Is Not Required to Make DCVs

(A) Electron microscopy of synapses in the ventral nerve cord of wild-type and *rund-1(tm3622)*. White arrowheads point to DCVs. Black arrowheads point to the presynaptic density. Scale bar, 200 nm.

(B) Quantification of synaptic vesicles (SVs) and dense-core vesicles (DCVs) at synapses in the ventral cord (V) or dorsal cord (D). Values are represented as mean ± SEM.

B

Genotype	# profiles / animals	Mean synaptic area (μm^2)	SV / profile	Mean diameter of SVs (nm)	DCV / profile	Mean diameter of DCVs (nm)
wild type V	69/5	0.20 ± 0.01	32.9 ± 2.2	31.2 ± 0.4	2.1 ± 0.3	43.2 ± 0.5
rund-1(tm3622) V	31/2	0.17 ± 0.01	36.3 ± 2.3	30.4 ± 0.3	4.5 ± 0.6	43.5 ± 0.6
wild type D	11/2	0.17 ± 0.03	38.5 ± 4.0	30.9 ± 0.4	2.7 ± 0.8	43.6 ± 0.9
rund-1(tm3622) D	16/2	0.19 ± 0.02	36.2 ± 2.7	31.4 ± 0.5	5.3 ± 1.2	44.0 ± 1.2

Sumakovic et al., 2009; Figures S7B–S7D and data not shown). These data support a model in which the unmotivated class of proteins, RAB-2, RUND-1, and CCCP-1, act in parallel to EGL-3 to regulate locomotion, perhaps via different DCV cargos; both pathways may require UNC-31/CAPS for secretion.

RUND-1 and CCCP-1 Are Required to Sort Dense-Core Vesicle Cargo

To test whether *rund-1* affects synaptic or dense-core vesicle transport, we examined the ultrastructure of *rund-1(tm3622)* using electron microscopy. *rund-1* does not exhibit defects in synaptic vesicle number (Figure 3) or localization of synaptic vesicle cargo (Figures S5A and S5B). Nor is synaptic function defective in *rund-1* and *cccp-1* mutants as determined by electrophysiological recordings (Figures S5C–S5G). Also, DCVs of a normal size and appearance are present at synapses in both the ventral and dorsal nerve cords of the *rund-1(tm3622)* mutant (Figure 3). In fact, there is actually a small increase in the number of DCVs. Thus, RUND-1 is not required for synaptic vesicle or DCV biogenesis or transport to synapses. These data support the idea that RUND-1 and CCCP-1 are required for sorting of DCV cargos.

We tested whether *rund-1* and *cccp-1* play a role in DCV cargo trafficking. IDA-1 is the *C. elegans* ortholog of the DCV transmembrane protein phogrin (Cai et al., 2004). *rund-1* and *cccp-1* mutants exhibit a defect in axonal trafficking of IDA-1::GFP (Figure 4F), but it is weaker than that observed in *rab-2* mutants (Edwards et al., 2009).

We followed soluble components of DCVs by tagging the Venus fluorescent protein to the processed propeptides NLP-21 and FLP-3 and the nonprocessed peptide INS-22. During vesicle maturation, the processed propeptides are cleaved and the fluorescent protein is released within the vesicle. The mature vesicle is then transported into the axon. *rund-1* and *cccp-1* mutations reduced axonal fluorescence of Venus (Figures 4A–4C and 4E; Figure S6A). The loss of fluorescence in the axons was not caused by a defect in polarity since there was no increase of fluorescence in the dendrites (Figure 4D). Expression of the *rund-1* cDNA in the same cells fully rescued the *rund-1* trafficking defect (Figure 4C), indicating that RUND-1 acts cell autonomously.

rab-2 mutants show soluble cargo trafficking defects similar to *rund-1* and *cccp-1* mutants (Edwards et al., 2009; Sumakovic et al., 2009). To determine whether these genes act in the same pathway, we built double mutants and measured axonal fluorescence. In all cases, double mutants showed defects comparable to the single mutants (Figures 4A, 4B, and 4E), providing additional evidence that *rab-2*, *rund-1*, and *cccp-1* function in the same genetic pathway.

Despite the loss of soluble fluorescent proteins from vesicles in these mutants, neuropeptide trafficking into axons does not seem to be blocked. The Venus tag can be forced to remain with neuropeptides by mutation of the *egl-3* proprotein convertase. In the absence of the convertase, Venus cannot be cleaved from the condensed peptides. In the *rund-1 egl-3* double mutant, Venus-tagged NLP-21 and FLP-3 is observed in the axons (Figure 4C), as was previously observed in *rab-2 egl-3* double mutants (Edwards et al., 2009; Sumakovic et al., 2009). However, in both *rab-2 egl-3* and *rund-1 egl-3* double mutants, there is still a reduction in axonal fluorescence compared to *egl-3* single mutants (Edwards et al., 2009; Sumakovic et al., 2009; data not shown), suggesting that there is also reduced trafficking of unprocessed cargo in *rab-2* and *rund-1* mutants.

To assay the release of DCV cargo, we measured the accumulation of Venus fluorescence in coelomocytes, scavenger cells residing in the body cavity of the worm (Sieburth et al., 2007; Speese et al., 2007). *cccp-1* mutants have reduced fluorescence in coelomocytes, suggesting that missorted cargo is not released in *cccp-1* mutants. *rund-1* mutants lack fluorescence in axons but accumulate fluorescence in the coelomocytes at wild-type levels (Figure 4D), suggesting that an alternative release pathway in the cell body is still intact in *rund-1* mutants. This may be due to missorting of cargo to the constitutive secretory pathway.

RUND-1 and CCCP-1 Are Localized to the *trans*-Golgi in Neuronal Cell Bodies

The *rund-1* gene was tagged at its C terminus with GFP, tagRFP, or tdEos and inserted as a single copy in the genome. These constructs fully rescued the *rund-1* mutant locomotion defect

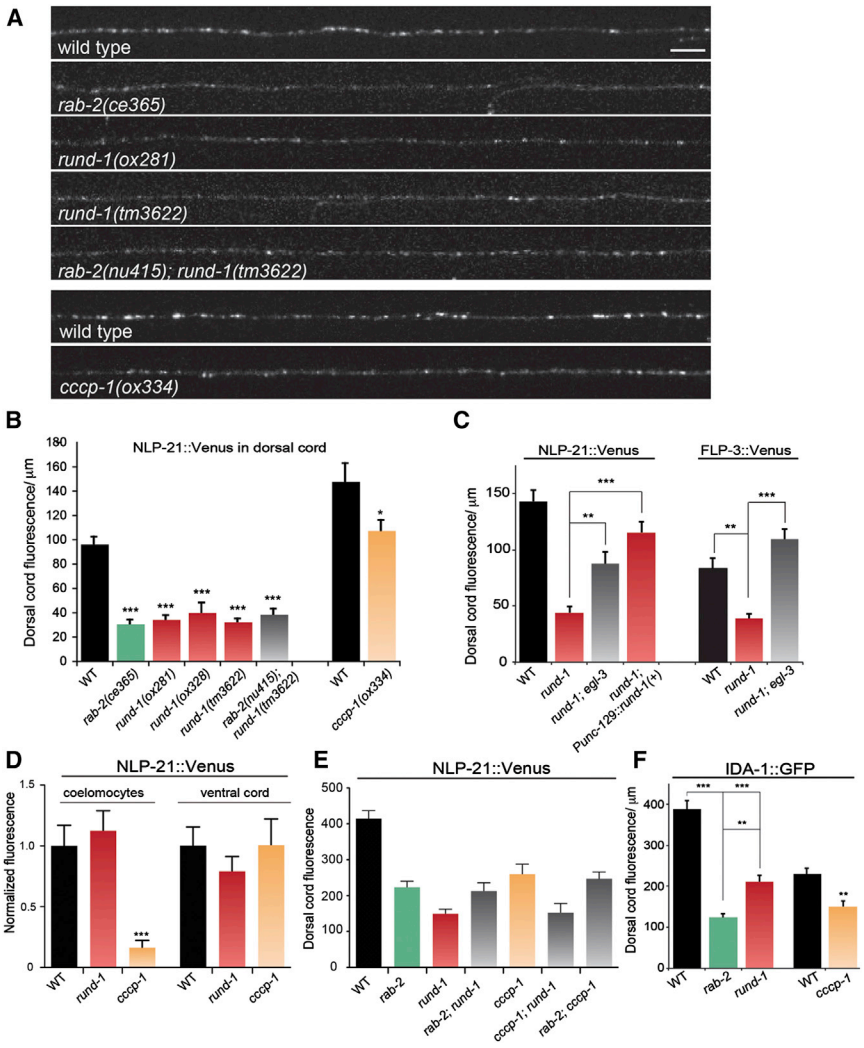

Figure 4. *rund-1* and *cccp-1* Mutants Have Defects in Trafficking DCV Cargos

(A) Images of NLP-21::Venus fluorescence in motor neuron axons of the dorsal nerve cord. *rab-2*, *rund-1*, and *cccp-1* mutants have decreased levels of fluorescence in the dorsal cord, indicative of an NLP-21::Venus trafficking defect. The final two panels (WT and *cccp-1*) were from a separate experiment. Scale bar, 5 µm.

(B) NLP-21::Venus fluorescence levels are decreased in the dorsal cord in *rab-2*, *rund-1*, and *cccp-1* mutants. The mean fluorescence intensity per µm is given in arbitrary units. All single mutants are defective in trafficking NLP-21::Venus to the dorsal cord (***$p < 0.001$; *$p < 0.05$ versus wild-type). The *rab-2 rund-1* double mutant is not significantly different from the single mutants ($p > 0.05$). Error bars, SEM; n = 9–22.

(C) Trafficking of NLP-21::Venus and FLP-3::Venus is rescued by *egl-3* mutants. The peptide processing mutant *egl-3* suppresses NLP-21::Venus and FLP-3::Venus trafficking defects of the *rund-1(tm3622)* mutant (**$p < 0.01$, ***$p < 0.001$, respectively). The *rund-1* NLP-21::Venus defect is rescued by expression of the wild-type *rund-1* cDNA in the dorsal motor neurons (***$p < 0.001$). Error bars, SEM; n = 6–11.

(D) Secreted NLP-21::Venus fluorescence levels in coelomocytes. *cccp-1(ox334)* has decreased coelomocyte fluorescence (***$p < 0.001$) but *rund-1(tm3622)* has no defect ($p > 0.05$). Neither *rund-1* nor *cccp-1* has decreased fluorescence in the ventral cord ($p > 0.05$). Error bars, SEM; n = 13–21.

(E) *rab-2*, *rund-1*, and *cccp-1* act in the same genetic pathway. Double mutants of *rab-2(nu415)*, *rund-1(tm3622)*, and *cccp-1(ox334)* are similar to single mutants in trafficking NLP-21::Venus to the dorsal cord ($p > 0.05$ for all pairwise comparisons except *cccp-1; rund-1* versus *cccp-1*, $p < 0.05$). All mutants exhibit significant defects compared to wild-type ($p < 0.001$). Error bars, SEM; n = 10–13.

(F) IDA-1::GFP fluorescence levels in the dorsal cord. The *rab-2(nu415)*, *rund-1(tm3622)*, and *cccp-1(ox334)* mutants are defective in trafficking IDA-1::GFP (***$p < 0.001$ and **$p < 0.01$ versus WT). Error bars, SEM; n = 9–13.

(Figure 2C; Figure S3E). RUND-1 localized mainly to two or three perinuclear puncta in neuronal cell bodies; only extremely faint fluorescence was observed in axons (Figure 5; Figure S8A).

We examined colocalization of RUND-1::tagRFP with GFP-tagged markers for various compartments (Figure 5A). All markers were expressed as single-copy insertions since overexpression of some markers can change the size of the corresponding compartment (Bucci et al., 1992, 2000). RUND-1 did not localize to compartments that communicate with the Golgi, including the ER (TRAM-1), the early endosome (RAB-5), recycling endosome (RAB-11.1), late endosome (RAB-7), or with the general endosome marker syntaxin-13 (SYN-13). RUND-1 showed partial overlap with a *cis*-Golgi marker (the COP I vesicle marker ε-COP) and more overlap with a medial-Golgi marker (AMAN-2, mannosidase II). In neuronal cell bodies, RUND-1 showed almost perfect colocalization with the *trans*-Golgi markers RAB-6.2 and syntaxin 6 (SYX-6). RAB-6.2 is localized predominantly to the *trans*-Golgi and is also found on exocytotic vesicles leaving the Golgi (Goud et al., 1990; Grigoriev et al., 2007); syntaxin 6 is a *trans*-Golgi SNARE also found on immature secretory granules in neuroendocrine cells (Bock et al., 1997; Klumperman et al., 1998). We conclude that RUND-1 localizes to the *trans*-Golgi or to vesicles closely associated with the *trans*-Golgi. Localization of RAB-6.2 and syntaxin 6 were not altered in a *rund-1* mutant background (data not shown), suggesting that *rund-1* is not required for normal Golgi structure.

To confirm that RUND-1 localized to the Golgi, we performed correlative nanometer-resolution fluorescence electron microscopy (Watanabe et al., 2011). Fluorescence from the tdEos-tagged RUND-1 was localized using superresolution PALM imaging and superimposed on scanning electron micrographs. RUND-1 was localized to the Golgi in neuronal cell bodies (Figure 5B) and in pharyngeal cells (data not shown).

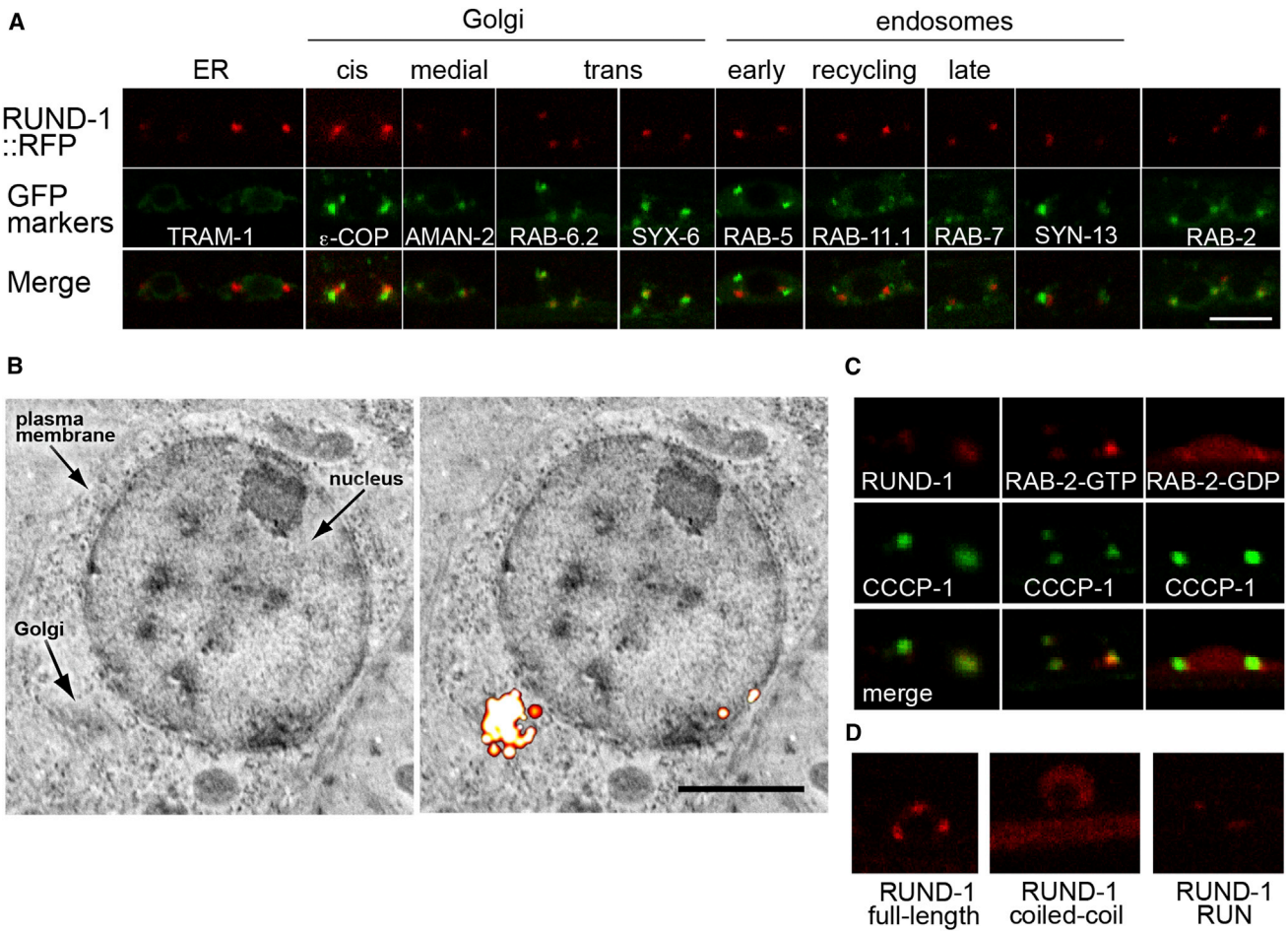

Figure 5. RUND-1 Colocalizes with RAB-2 at the *trans*-Golgi Network

(A) RUND-1 colocalizes with RAB-2 and *trans*-Golgi markers. Each panel shows a single slice of a confocal image of motor neuron cell bodies in the ventral cord of young adult animals. The top boxes show the localization of a single-copy rescuing RUND-1::tagRFP-T fusion protein (*oxIs590*). RUND-1 localizes almost exclusively to two or three perinuclear puncta per cell. The middle boxes show the localization of single-copy GFP-tagged compartment markers. The bottom boxes show the merged images. Scale bar, 5 μm, applies to all panels. RUND-1 shows tightest colocalization with RAB-6.2, a *trans*-Golgi Rab protein, and with SYX-6, the ortholog of the *trans*-Golgi SNARE syntaxin 6. RUND-1 puncta also colocalize well with RAB-2 puncta. RUND-1 partially overlaps with the medial-Golgi marker mannosidase II (AMAN-2) and the *cis*-Golgi marker εCOP. RUND-1 is not colocalized with the rough ER marker TRAM-1 or with the endosomal markers RAB-5, RAB-11.1, RAB-7, and SYN-13.

(B) RUND-1 localizes to the Golgi. Left: a backscatter scanning electron micrograph of the cell body of a neuron in the nerve ring. Right: the same image overlaid with the corresponding fluorescence PALM image of RUND-1::tdEos. Scale bar, 1 μm.

(C) CCCP-1 colocalizes with RUND-1 and RAB-2. CCCP-1 colocalizes with RUND-1 and RAB-2(GTP). CCCP-1 is still punctate when coexpressed with RAB-2(GDP), which is diffusely expressed.

(D) The RUN domain of RUND-1 mediates its localization. Full-length RUND-1, the coiled-coil domain, and the RUN domain were tagged at their C termini with tagRFP-T and integrated in the genome. The truncated proteins were expressed at lower levels. See also Figure S8.

To determine which part of RUND-1 mediates its localization, we split RUND-1 into two pieces and tagged each with tagRFP. The coiled-coil domain of RUND-1 was spread diffusely throughout the cell body and axons (Figure 5D). In contrast, the RUN domain of RUND-1 was sufficient for localization to perinuclear puncta (Figure 5D). Neither truncation rescued a *rund-1* mutant, suggesting that both domains are required for normal function but that the RUN domain is sufficient for localization.

We also tagged CCCP-1 with GFP and expressed it using the P*rab-3* neuronal promoter. CCCP-1 is localized mainly to perinuclear puncta in neuronal cell bodies (Figure 5C) but unlike RUND-1 is also more diffusely spread throughout cell bodies and axons. This pattern resembles that of RAB-2 (Edwards et al., 2009; Sumakovic et al., 2009). To confirm the broader localization of RAB-2, we inserted a GFP::RAB-2 single-copy transgene in the genome (Figure S8C). Like CCCP-1, RAB-2 was found at perinuclear puncta and also diffusely in the cell body and axons. RUND-1 and RAB-2 colocalize at perinuclear puncta in neuronal cell bodies (Figure 5A).

The localization of RUND-1 and CCCP-1 to the Golgi is not disrupted in *rab-2* mutants (Figures S8A, S8B, S8D, and S8E), nor is

CCCP-1 localization affected by GTP-bound or GDP-bound RAB-2 (Figure 5C). Conversely, RAB-2 is not mislocalized in *rund-1* and *cccp-1* mutants (Figure S8C). Finally, RUND-1 is localized normally in a *cccp-1* mutant and CCCP-1 is localized normally in a *rund-1* mutant (Figures S8A and S8B). Thus, RUND-1, CCCP-1, and RAB-2 are not required for each other's localization.

RUND-1 and CCCP-1 Bind RAB-2 Specifically

Using yeast two-hybrid assays, we examined the interactions of full-length RUND-1 and CCCP-1 with three different forms of RAB-2: (1) the constitutively active GTP-bound form RAB-2(Q65L), (2) the constitutively inactive GDP-bound form RAB-2(S20N), and (3) the wild-type RAB-2. RUND-1 interacted with GTP-bound RAB-2 but not with the GDP-bound RAB-2 or the wild-type RAB-2 (Figure 6A). Thus, like other RUN-domain proteins, the interaction of RUND-1 with RAB-2 is specific to the activated GTP-bound form of the Rab. CCCP-1 interacted with both the GTP-bound and wild-type RAB-2 but not with the GDP-bound RAB-2 (Figure 6A). This suggests a stronger interaction of RAB-2 and CCCP-1 that is still GTP dependent, given that some of the wild-type RAB-2 is expected to be GTP bound. RUND-1 and CCCP-1 did not interact with each other in two-hybrid assays (data not shown).

To test for specificity of these interactions, we performed yeast two-hybrid assays with RUND-1 or CCCP-1 and GTP-bound versions of other members of the Rab, Rap, Ras, and Ral families of small GTPases. RUND-1 and CCCP-1 showed an interaction only with RAB-2 (Figure 6B; data not shown). Thus, RUND-1 and CCCP-1 are specific RAB-2 interactors.

We split RUND-1 into two pieces and assayed binding to RAB-2. The coiled-coil domain fragment did not interact with GTP-bound RAB-2. The RUN domain fragment interacted robustly with GTP-bound RAB-2 (Figure 6C). This construct carries the entire RUN domain and a putative upstream α-helix that is needed for proper folding of other RUN domains (Kukimoto-Niino et al., 2006; Recacha et al., 2009). A shorter construct lacking the upstream α-helix and the beginning of the conserved A block of the RUN domain did not show an interaction with RAB-2 (data not shown). Thus, it seems likely that the RUN domain is required for the interaction of RUND-1 with RAB-2.

RUND-1 Binds RIC-19 and TBC-8

RAB-2 binds TBC-8, a putative RAB-2 GAP, and RIC-19, a BAR domain protein (Hannemann et al., 2012; Sumakovic et al., 2009). RUND-1 also interacts with TBC-8 in yeast two-hybrid assays and with both TBC-8 and RIC-19 when coexpressed in HEK293 cells (Figures 6D and 6E). In contrast, CCCP-1 did not interact with TBC-8 or RIC-19 in two-hybrid assays (data not shown). Thus, RUND-1, but not CCCP-1, independently binds RAB-2 and other RAB-2 partners including RIC-19 and TBC-8.

TBC-8 consists of an N-terminal RUN domain and a C-terminal TBC domain responsible for the GAP activity. A fragment of TBC-8 carrying its RUN domain binds RUND-1, but fragments carrying only the TBC GAP domain do not bind (Figures 6E and 6F). The TBC-8 RUN domain also binds RIC-19 (Hannemann et al., 2012). The RUND-1 coiled-coil domains do not interact with TBC-8, but the RUND-1 RUN domain exhibited a weak interaction with TBC-8 (data not shown). Thus, RUND-1 and TBC-8 interact via regions containing their RUN domains.

To determine whether *ric-19* and *tbc-8* exhibit genetic interactions with *rund-1*, we built double mutants and assayed locomotion and DCV cargo trafficking. Although *ric-19* had little effect on locomotion on its own (Sumakovic et al., 2009), it significantly enhanced the locomotion defect of *rund-1* (Figure 2G). Similarly, *ric-19* enhanced the NLP-21::Venus trafficking defect of *rund-1* (Figure S6B). These data indicate that RIC-19 acts in parallel to RUND-1, possibly as two distinct effectors of RAB-2. *tbc-8* mutants also have defects in sorting vesicle cargo (Hannemann et al., 2012). However the sorting defects in *rund-1* mutants were not enhanced in *rund-1 tbc-8* double mutants (Figure S6B), indicating that *tbc-8* and *rund-1* act in the same pathway.

DISCUSSION

We performed a genetic screen for mutants defective in dense-core vesicle function and identified two proteins, RUND-1 and CCCP-1. RUND-1 and CCCP-1 are required for proper sorting of DCV cargo but are not required for DCV morphology or transport. Genetic and biochemical data show that these proteins are probably Rab2 interactors at the *trans*-Golgi. RUND-1 also interacts with the BAR domain protein RIC-19 and the RAB-2 GAP TBC-8, both of which individually interact with RAB-2. These results identify a set of interacting proteins that function in the trafficking of DCV cargos.

RUND-1 and CCCP-1 Interact with RAB-2 at the Golgi

The function of a Rab protein is defined by its localization to a specific cellular compartment and by its effector proteins. Rab2 was originally localized to the ER-Golgi intermediate compartment (Chavrier et al., 1990) and was thought to function in ER-to-Golgi anterograde trafficking (Tisdale et al., 1992), but Rab2 is distributed more broadly across the Golgi and may have additional roles (Chun et al., 2008; Sumakovic et al., 2009). Known effectors of Rab2 include several coiled-coil proteins associated with the Golgi (Hayes et al., 2009; Short et al., 2001; Sinka et al., 2008) and the BAR domain protein ICA69/RIC-19 (Buffa et al., 2008; Sumakovic et al., 2009).

Here we demonstrate that the RUN domain protein RUND-1 and the conserved coiled-coil protein CCCP-1 are possible novel effectors of RAB-2. Five lines of evidence support this conclusion. First, *rund-1*, *cccp-1*, and *rab-2* mutants exhibit a similar locomotory phenotype. Second, *rund-1*, *cccp-1*, and *rab-2* mutants exhibit similar defects in trafficking DCV cargo. Third, *rund-1*, *cccp-1*, and *rab-2* act in the same genetic pathway. Fourth, RUND-1, CCCP-1, and RAB-2 colocalize at the *trans*-Golgi network. Fifth, RUND-1 and CCCP-1 bind to the active GTP-bound form of RAB-2 but not the inactive GDP-bound form.

Classical Rab effectors are recruited to a compartment by binding to the active GTP-bound Rab. For example, RIC-19 is recruited to the Golgi by GTP-RAB-2 and dispersed into the cytoplasm by GDP-RAB-2 (Sumakovic et al., 2009). However, neither RUND-1 nor CCCP-1 localization is dependent on RAB-2. RUND-1 localization is mediated by its RUN domain but independently of RAB-2 binding. Recently, the RAB-10 effector

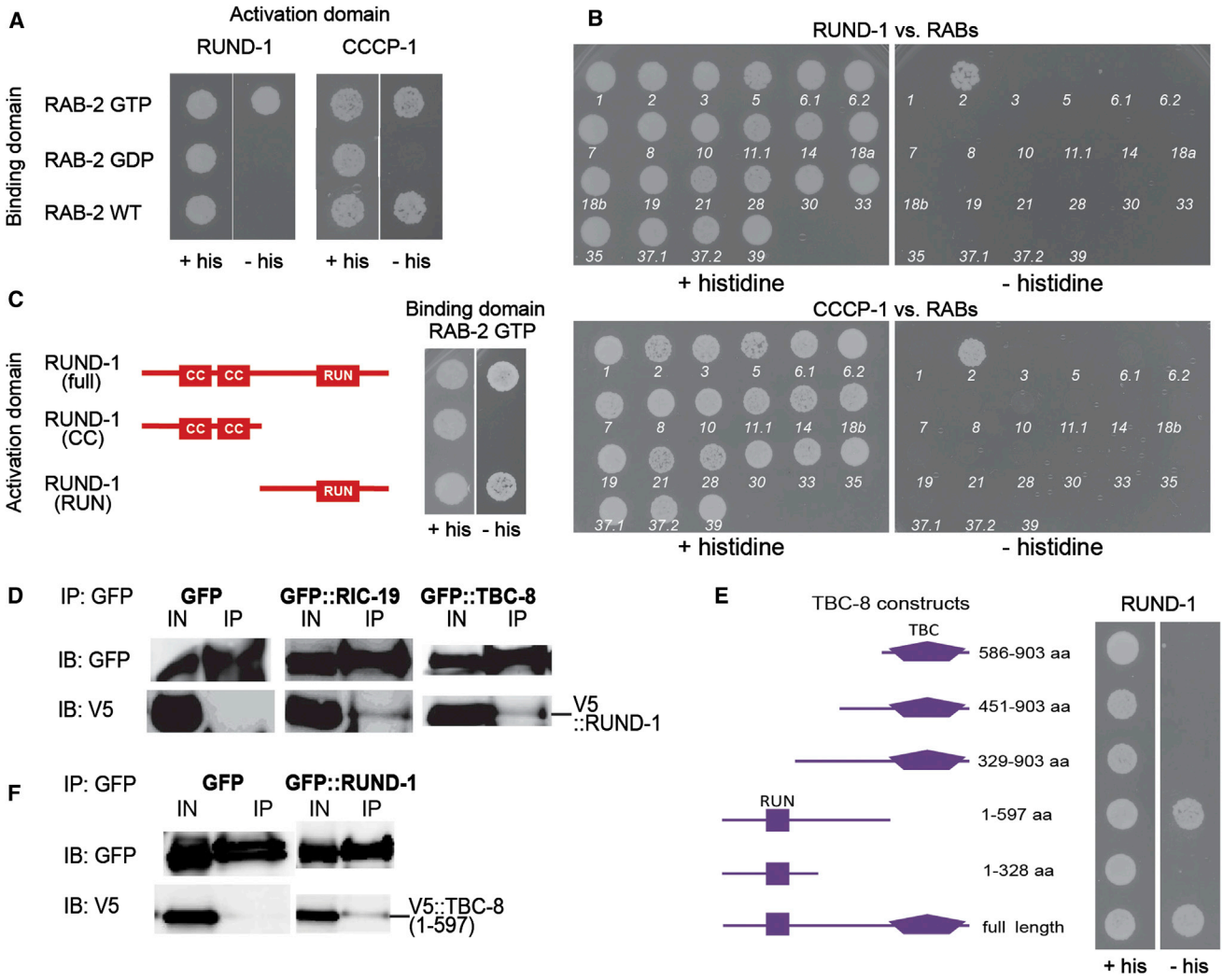

Figure 6. RUND-1 and CCCP-1 Interact Physically with Activated RAB-2

(A) RUND-1 interacts specifically with GTP-bound RAB-2 (RAB-2 GTP) in a yeast two-hybrid assay. RUND-1 did not show an interaction with wild-type RAB-2 (RAB-2 WT) or inactive GDP-bound RAB-2 (RAB-2 GDP). CCCP-1 interacts with RAB-2 GTP and RAB-2 WT, but not with RAB-2 GDP. Growth without histidine (– his) indicates a physical interaction.

(B) The RUND-1 and CCCP-1 interactions with RAB-2 are specific. The interactions of RUND-1 and CCCP-1 with *C. elegans* RAB proteins were examined by yeast two hybrid. Numbers indicate the number of the RAB gene in *C. elegans* (e.g., 1 = RAB-1). RUND-1 and CCCP-1 interact only with RAB-2. RAB-27 could not be tested because of self-activation.

(C) RUND-1 interacts with RAB-2 via the RUN domain. Two truncations of RUND-1 were used: RUND-1 (CC) consists of amino acids 1–261 and RUND-1 (RUN) consists of amino acids 262–549.

(D) RUND-1 interacts with RIC-19 and TBC-8. V5-tagged RUND-1 was coexpressed with GFP, GFP::RIC-19, or GFP::TBC-8 in HEK293 cells. Immunoprecipitation of GFP::RIC-19 or GFP::TBC-8 pulled down RUND-1. Immunoprecipitation of untagged GFP did not pull down RUND-1. IN, input; IP, immunoprecipitation; IB, immunoblotting.

(E) RUND-1 interacts with TBC-8 outside of its TBC domain. Truncations of TBC-8 were examined for interactions with RUND-1 by yeast two hybrid.

(F) RUND-1 interacts with TBC-8 outside of its TBC domain. V5-tagged TBC-8 (1–597 aa) was coexpressed with GFP or GFP::RUND-1 in HEK293 cells. Immunoprecipitation of GFP::RUND-1 pulled down TBC-8 (1–597). IN, input; IP, immunoprecipitation; IB, immunoblotting.

EHBP-1 has been shown instead to mediate localization of its cognate Rab (Shi et al., 2010). However, RAB-2 localization does not depend on either RUND-1 or CCCP-1. Nor are RUND-1 and CCCP-1 required for each other's localization. Thus, RUND-1, CCCP-1, and RAB-2 all appear to localize independently or have multiple binding partners at the Golgi.

RUND-1 Is a Member of the RUN Domain Protein Family

RUN domain proteins were originally proposed to be potential Rab and Rap effectors (Callebaut et al., 2001). Clear physical interactions with Rab and Rap proteins have been shown for some of these proteins (Bayer et al., 2005; Cormont et al., 2001; Fouraux et al., 2004; Janoueix-Lerosey et al., 1995,

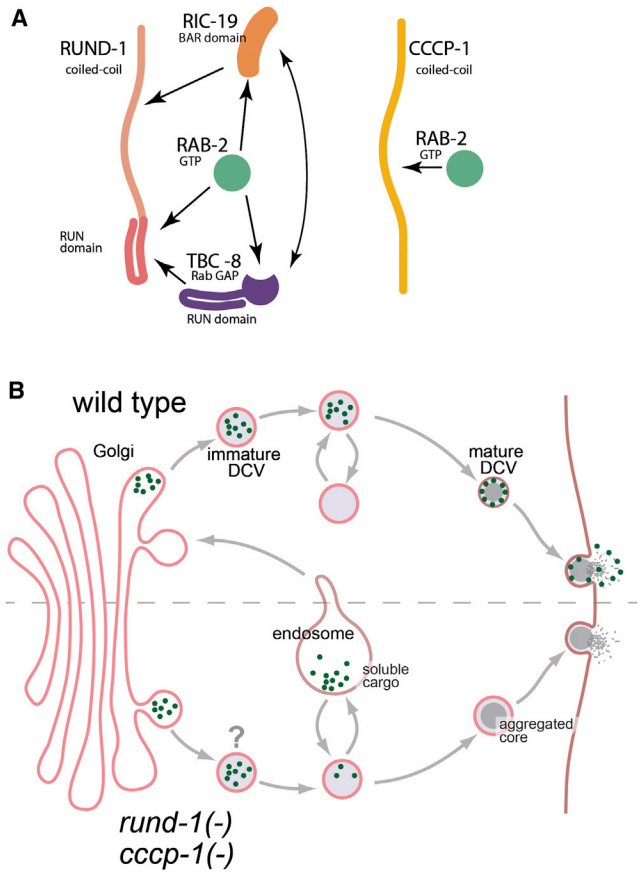

Figure 7. Model for RUND-1 and CCCP-1 Action in DCV Maturation

(A) RUND-1 may be in a complex with activated RAB-2, RIC-19, and TBC-8 since all of these molecules bind each other in pairwise combinations. CCCP-1 binds activated RAB-2 but does not bind RUND-1, RIC-19, or TBC-8, so it may be in a separate complex.

(B) RUND-1 and CCCP-1 localize near the *trans*-Golgi and are involved in regulating cargo sorting during the formation of mature DCVs. Soluble cargo (green dots) are retained in the mature vesicle and released at the plasma membrane. In the absence of *rund-1* and *cccp-1*, immature DCVs may have an improper identity (denoted by "?"), causing them to lose soluble cargo to the endolysosomal system. However, insoluble cargo is not lost, including peptides that aggregate and form the characteristic dense core seen by EM. The process of aggregation is depicted as a gradual graying and condensation of the vesicle center during the maturation process. Though axonally localized DCVs carry reduced amounts of certain cargos in *rund-1* mutants, overall release is normal as assayed by coelomocyte uptake, suggesting that the "lost" cargos are still secreted, perhaps as a result of their missorting to the constitutive secretory pathway. In *cccp-1* and *rab-2* mutants, release of such cargos is reduced, suggesting that they may be misdirected to the lysosome and degraded.

1998; Kukimoto-Niino et al., 2006; Miserey-Lenkei et al., 2007; Recacha et al., 2009). Moreover, the crystal structure of the RUN domain of Rab6 IP1 in complex with Rab6 provides evidence that the RUN domain is sufficient to mediate binding to Rabs in at least some cases (Recacha et al., 2009). However, there are few functional studies that tie RUN domains to Rab function. Our data provide in vivo support to the conclusion that RUN domains mediate Rab protein functions.

We demonstrate that the RUN domain of RUND-1 is sufficient to interact with RAB-2. Like for other RUN domains, this interaction is specific to GTP-bound RAB-2. Moreover, RAB-2 is probably the only small GTPase that interacts with RUND-1. Most RUN domain proteins studied interact with at most a single Rab protein, although this has not been exhaustively analyzed (Bayer et al., 2005; Fukuda et al., 2011; Miserey-Lenkei et al., 2007; Recacha et al., 2009). A recent genome-wide analysis detected Rab interactors for only six of 19 mammalian RUN domain proteins by yeast two-hybrid assays (Fukuda et al., 2011). However, this study did not detect an interaction between the mammalian orthologs of RUND-1 and RAB-2, so it is possible that weaker interactions were missed.

In addition to the RUN domain, most RUN domain proteins have other interaction domains (Callebaut et al., 2001). RUND-1 has two N-terminal coiled-coil domains. Coiled-coil domains typically mediate protein-protein interactions and are especially common in RUN domain proteins (Cormont et al., 2001; Fouraux et al., 2004; Janoueix-Lerosey et al., 1998; Lan et al., 2005; Matsunaga et al., 2009; Mori et al., 2007; Yang et al., 2002; Zhong et al., 2009). Unlike the coiled-coil domains of some Rab effectors such as the golgins (Burguete et al., 2008; Hayes et al., 2009; Short et al., 2001; Sinka et al., 2008), the coiled-coil domains of RUND-1 are not required for binding to RAB-2. However, the coiled-coil domains of RUND-1 are conserved, and the *ox328* missense mutation in the second coiled-coil domain is a severe allele. It seems likely that the coiled-coil domains of RUND-1 mediate important interactions with other proteins acting in the RAB-2 pathway.

Function of RAB-2 and Its Interactors

RAB-2 appears to have at least three interacting proteins in the DCV maturation pathway: RUND-1, CCCP-1, and RIC-19. These proteins could act separately as independent interactors of RAB-2, or they could act together in a single complex. The data are consistent with the possibility that RAB-2 forms a single complex with RUND-1, RIC-19, and TBC-8 since these proteins exhibit direct pairwise interactions and are colocalized at the Golgi (Figure 7A). In contrast, CCCP-1 interacts only with RAB-2 and may act as an independent effector. Interestingly, the locomotion and DCV cargo trafficking phenotypes of *rab-2*, *rund-1*, and *cccp-1* are similar but not identical, indicating that there are distinct functions for each protein. The locomotion and trafficking defects of *rund-1* and *cccp-1* mutants are generally weaker than the *rab-2* mutant defects, indicating that RUND-1 and CCCP-1 may participate in only certain aspects of RAB-2 function or to only a partial degree. Also, *rund-1* mutants do not impair cargo secretion as assayed by coelomocyte uptake, suggesting a different final destination for missorted cargos in *rund-1* mutants versus *cccp-1* and *rab-2* mutants (Sumakovic et al., 2009). However, the overt phenotypic similarities of these mutants as well as the genetic interactions suggest that these proteins act in the same process during cargo sorting into DCVs.

The primary cellular defect that we observe in these mutants is the reduced trafficking of fluorescent proteins targeted to DCVs, with no major effects on the morphology or transport of vesicles themselves. It is not clear which class of cargo accounts for the behavioral defects. The fact that the locomotion defects of *rab-2*,

Table 1. Mutants Isolated as Gq Suppressors

Gene	Protein	Function	Number of Alleles
egl-30	Gq alpha	Gq-alpha GTPase	6
ric-8	synembryn	G-protein GEF	1
egl-8	PLCbeta	Gq effector, DAG synthesis	4
unc-13	Munc13	DAG binding, MUN domain, SV + DCV exocytosis	1
unc-31	CAPS	MUN domain, DCV exocytosis	6
pkc-1	Protein kinase C	DAG binding, DCV exocytosis	1
unc-73	Trio	Gq-alpha effector, Rho GEF	2
rund-1	Rundc1	Golgi Rab2 effector	2
cccp-1	C10orf118	Golgi Rab2 effector	1
13 others	–	–	15

rund-1, and *cccp-1* mutants are enhanced by mutations in the proprotein convertase *egl-3* indicates that the behaviorally relevant missorted cargos are not processed by EGL-3 but rather may be peptides processed by other convertases or cargos that do not require processing at all.

What are the functions of RAB-2, RUND-1, and CCCP-1 at the Golgi during maturation of DCVs? There are several possibilities, not all mutually exclusive, such as specifying vesicle identity, tethering, budding, or cargo sorting. First, vesicle identity is often conveyed by Rab proteins (Stenmark, 2009), and RAB-2 and its interactors could provide identity to maturing DCVs. In the absence of markers of identity, the vesicles may become endosomal in character and fuse with the endolysosomal system, thereby losing some of their cargos (Figure 7B). Second, RUND-1 and CCCP-1 may tether vesicles via the "tentacular matrix" that moves vesicles processively through the Golgi (Munro, 2011; Sinka et al., 2008; Yu and Hughson, 2010). The tentacular matrix is posited to be formed by the golgins, long coiled-coil proteins that localize to the Golgi and capture vesicles by binding Rab proteins. Third, RUND-1 may act directly in the formation of vesicles. RUND-1 and RAB-2 interact with RIC-19, which contains a crescent-shaped BAR domain that may induce membrane curvature (Frost et al., 2009). Finally, RAB-2 and its interactors could be involved more directly in sorting. Since none of the proteins have a transmembrane domain, they are unlikely to serve as a sorting receptor per se but may be involved in the retrograde retrieval of a sorting receptor.

The possible RUND-1 complex may consist not only of the RAB-2 interactors RIC-19 and RUND-1 but the RAB-2 GAP protein TBC-8, which should turn off the Rab. The combination of positive and negative factors suggests that the complex may be quite dynamic. The binding of interactors to RAB-2 may simultaneously recruit the GAP that will hydrolyze GTP and cause dissolution of the complex. Such fine temporal control of RAB-2 activation may help deliver vesicles to their *trans*-Golgi acceptor and then release them from the acceptor complex as maturation proceeds.

The human ortholog of RUND-1 is RUNDC1, which is highly conserved in both the coiled-coil and RUN domains. When RUNDC1 is expressed in *rund-1* mutants, the human protein is localized to the Golgi and rescues the mutant phenotype, indicating a strong conservation of function. Human RUNDC1 has been identified as an inhibitor of the tumor suppressor p53 (Llanos et al., 2006), and RUNDC1 expression is used as a prognostic marker of metastasis in breast cancer tumors (van 't Veer et al., 2002). Thus, RUNDC1 is a possible oncogene. RUNDC1 has not been reported to have any function in the nervous system but maps to chromosomal position 17q21, in the same region of a likely autism gene (Cantor et al., 2005). An individual with autism has also been found to carry a de novo nonsense mutation in Rab2A, the human ortholog of RAB-2 (Sanders et al., 2012). Because *Rundc1* and *Rab2A* are expressed in the mouse brain (Allen Brain Atlas), it is possible that RUND-1 and its interactors function in DCV cargo trafficking in the vertebrate brain as well as in nematodes.

EXPERIMENTAL PROCEDURES

Strains

Worm strains were cultured and maintained using standard methods (Brenner, 1974). A complete list of strains and mutations used is provided in the Supplemental Experimental Procedures.

Screen for Suppressors of Activated Gq

egl-30(tg26) encodes an activating mutation in Gαq. We mutagenized *egl-30(tg26)* worms with 0.5 mM ENU (*N*-ethyl-*N*-nitrosourea) for 4 hr as described in De Stasio and Dorman (2001). We screened the F_2 generation for suppression of the hyperactive locomotion phenotype of *egl-30(tg26)*. From screens of ~18,000 mutagenized haploid genomes, we isolated 43 mutants. Most of these mutants suppressed not only the hyperactivity of *egl-30(tg26)* but also the small size and slower growth rate, indicating that they specifically suppress Gq and do not affect locomotory function indirectly. To more generally test for the specificity of suppression, we built double mutants between *egl-30(tg26)* and a number of mutations that impair movement by affecting function of the neuromuscular junction: the N-type calcium channel *unc-2*, the synaptic vesicle docking/priming protein *unc-18*, the synaptic vesicle kinesin *unc-104*, the ryanodine receptor *unc-68*, the proprotein convertase *egl-3*, and the acetylcholine receptor assembly factors *unc-50* and *unc-74*. In all cases, the double mutants exhibited phenotypes that resembled a combination of the two individual mutants, indicating additive effects with *egl-30(tg26)*. Locomotion rates were reduced, but double mutants were uncoordinated, small, and slower growing than either of the parents. Thus, general disruptions of neuronal or muscular function do not nonspecifically suppress *egl-30(tg26)*.

We mapped 39 of the suppressors and assigned them to 22 different complementation groups (Table 1). Several were known to act in the Gq pathway, including loss-of-function mutations in *egl-30*/Gqα, *ric-8*/Gα GEF, *unc-73*/Trio, *egl-8*/phospholipase Cβ, and the DAG-binding synaptic protein UNC-13. Others included genes thought to be involved in DCV secretion, including *unc-31*/CAPS, and *pkc-1*/protein kinase C (Sieburth et al., 2007). The remaining 18 unidentified mutants comprised 15 complementation groups with one or two alleles each. Mutants in six genes had a strong unmotivated locomotion phenotype. We characterized two of these in detail, *rund-1* and *cccp-1*.

Mapping and Cloning *rund-1* and *cccp-1*

The *rund-1(ox281)* mutation was mapped to the left arm of chromosome X using SNPs in the Hawaiian strain CB4856 (Davis et al., 2005). Fine mapping, facilitated by picking recombinants between *rund-1(ox281)* and *dpy-3*, narrowed the *rund-1* interval to a 60 kb region with nine predicted genes, most on cosmid T19D7. Injection of cosmid T19D7 into *rund-1(ox281)* rescued the mutant phenotype. RNAi of the gene T19D7.4 caused a defecation defect reminiscent of *rund-1* mutants. We sequenced the T19D7.4 gene in the *rund-1* mutants *ox281* and *ox328*. *rund-1(ox281)* is a G to A transition in the splice acceptor of the sixth intron. *rund-1(ox328)* is an A to C transversion

that causes a T237P missense mutation in the second coiled-coil domain. We rescued *rund-1* mutants with a transgene containing only T19D7.4, confirming the gene identification.

The *cccp-1(ox334)* mutation was mapped to a 126 kb region on the left arm of chromosome III with 16 predicted genes. Because no *C. elegans* cosmids covered this region, we obtained two *C. briggsae* BACs (from CHORI) carrying orthologs of the genes in this region and injected them into *cccp-1(ox334)* mutants. The BAC RPCI94_09N13 rescued the *cccp-1* locomotion defect, while the BAC RPCI94_26P21 did not. RPCI94_09N13 carries orthologs of two *C. elegans* genes in this region, Y49E10.23 and Y49E10.24. Both *cccp-1* alleles introduce early stop mutations in Y49E10.23: *cccp-1(ox334)* carries a T to A transversion in exon 7 and *cccp-1(e1122)* carries a C to T transition in exon 9, leading to stop mutations at L343 and Q482, respectively. We subsequently rescued *cccp-1(ox334)* with a transgene containing only Y49E10.23.

Locomotion Assays

We performed tracking assays by videotaping worms and processing the movies using a custom-made plugin for ImageJ (White et al., 2007). Assays were initiated by transferring three to five well-fed worms with a platinum worm pick to a tracking plate with a spot of food. Movies were taken for 30 min. For the rare periods in which a worm left the food, the data were omitted. For all experiments except the tissue-specific rescue of *rund-1*, data were collected on 2 different days for each strain and combined. There was no significant day-to-day variation.

To measure stimulated locomotion on food, body bends were counted in the first 2 min after placing animals on thin lawns of bacteria. A body bend was defined as the movement of the tail from maximum to minimum amplitude of the sine wave (Miller et al., 1999). For heatshock expression, animals were exposed to 34° for 1 hr and assayed 24 hr later as adults. To measure locomotion in liquid, we assayed thrashing as described in Hobson et al. (2011). We placed animals in a drop of M9 on an unseeded plate, waited for 1 min, and then counted thrashes for 90 s. A thrash was defined as a change in the direction of the bend in the middle of the animal. All body bending and thrashing assays were performed on at least 2 different days for each set of strains, but each graph shows the data from a single representative experiment.

Imaging and Image Analysis

Worms were mounted on 2% agarose pads and anesthetized with 50 mM sodium azide. Images were obtained using a Zeiss Pascal confocal microscope, a Leica SP2 confocal microscope, or a Nikon 80i wide-field compound microscope. To image the dorsal or ventral nerve cords, we oriented young adult animals with dorsal or ventral side up by exposure to the anesthetic for 10 min on the slide before placing the coverslip. For quantitative imaging of dorsal cord fluorescence, all strains in a given experiment were imaged on the same days and all microscope settings were kept constant. The same section of the dorsal cord posterior of the vulva was imaged in all worms. Maximum intensity projections were quantified using ImageJ software, measuring the total fluorescence in a region of interest encapsulating the cord and subtracting the background fluorescence of a region of identical size adjacent to the cord. For colocalization images, Pearson's correlation coefficients were calculated using Nikon Elements software by selecting a circular region of interest around individual cell bodies in the ventral cord.

Statistics

p values were determined using InStat 3.1a and GraphPad Prism 5.0d (GraphPad Software). Data sets were analyzed by a one-way ANOVA to test for differences among the set followed by a Bonferroni posthoc test to examine selected comparisons, or by the Kruskal-Wallis nonparametric ANOVA to test for differences among the set followed by Dunn's test to examine selected comparisons. For categorical data, we calculated a two-sided p value using Fisher's exact test.

For other methods see Supplemental Experimental Procedures.

ACCESSION NUMBERS

The GenBank accession numbers for the full-length sequences of the *rund-1* and *cccp-1b* transcripts reported in this paper are JN986879 and JN986880.

SUPPLEMENTAL INFORMATION

Supplemental Information includes Supplemental Experimental Procedures, eight figures, two tables, and four movies and can be found with this article online at http://dx.doi.org/10.1016/j.neuron.2014.02.017.

ACKNOWLEDGMENTS

We thank K. Iwasaki, K. Miller, J. Kaplan, Z. Zhou, S. Mitani, B. Grant, C. Frøkjær-Jensen, G. Hollopeter, and P. McEachern for strains and plasmids; Y. Kohara for cDNA clones; the Sanger Center for cosmids; R. Rawson for help with confocal microscopy; D. Hobson for data analysis algorithms; and I. Topalidou for comments on the manuscript. Strains were provided by the CGC (P40 OD010440). M.A. was supported by Helen Hay Whitney and by NIH R00MH082109. M.H. was supported by the University of Göttingen GGNB program (DFG grant GSC 226/1). S.E. was supported by German Research Foundation CMPB and the European Neuroscience Institute. This work was supported by NIH NS034307 and NSF IOS-0920069 to E.M.J.

Accepted: January 23, 2014
Published: April 2, 2014

REFERENCES

Ahras, M., Otto, G.P., and Tooze, S.A. (2006). Synaptotagmin IV is necessary for the maturation of secretory granules in PC12 cells. J. Cell Biol. *173*, 241–251.

Ailion, M., Inoue, T., Weaver, C.I., Holdcraft, R.W., and Thomas, J.H. (1999). Neurosecretory control of aging in Caenorhabditis elegans. Proc. Natl. Acad. Sci. USA *96*, 7394–7397.

Ann, K., Kowalchyk, J.A., Loyet, K.M., and Martin, T.F. (1997). Novel Ca2+-binding protein (CAPS) related to UNC-31 required for Ca2+-activated exocytosis. J. Biol. Chem. *272*, 19637–19640.

Avery, L., Bargmann, C.I., and Horvitz, H.R. (1993). The Caenorhabditis elegans unc-31 gene affects multiple nervous system-controlled functions. Genetics *134*, 455–464.

Bastiani, C.A., Gharib, S., Simon, M.I., and Sternberg, P.W. (2003). Caenorhabditis elegans Galphaq regulates egg-laying behavior via a PLCbeta-independent and serotonin-dependent signaling pathway and likely functions both in the nervous system and in muscle. Genetics *165*, 1805–1822.

Bayer, M., Fischer, J., Kremerskothen, J., Ossendorf, E., Matanis, T., Konczal, M., Weide, T., and Barnekow, A. (2005). Identification and characterization of Iporin as a novel interaction partner for rab1. BMC Cell Biol. *6*, 15.

Bock, J.B., Klumperman, J., Davanger, S., and Scheller, R.H. (1997). Syntaxin 6 functions in trans-Golgi network vesicle trafficking. Mol. Biol. Cell *8*, 1261–1271.

Borgonovo, B., Ouwendijk, J., and Solimena, M. (2006). Biogenesis of secretory granules. Curr. Opin. Cell Biol. *18*, 365–370.

Brenner, S. (1974). The genetics of Caenorhabditis elegans. Genetics *77*, 71–94.

Brundage, L., Avery, L., Katz, A., Kim, U.J., Mendel, J.E., Sternberg, P.W., and Simon, M.I. (1996). Mutations in a C. elegans Gqalpha gene disrupt movement, egg laying, and viability. Neuron *16*, 999–1009.

Bucci, C., Parton, R.G., Mather, I.H., Stunnenberg, H., Simons, K., Hoflack, B., and Zerial, M. (1992). The small GTPase rab5 functions as a regulatory factor in the early endocytic pathway. Cell *70*, 715–728.

Bucci, C., Thomsen, P., Nicoziani, P., McCarthy, J., and van Deurs, B. (2000). Rab7: a key to lysosome biogenesis. Mol. Biol. Cell *11*, 467–480.

Buffa, L., Fuchs, E., Pietropaolo, M., Barr, F., and Solimena, M. (2008). ICA69 is a novel Rab2 effector regulating ER-Golgi trafficking in insulinoma cells. Eur. J. Cell Biol. *87*, 197–209.

Burguete, A.S., Fenn, T.D., Brunger, A.T., and Pfeffer, S.R. (2008). Rab and Arl GTPase family members cooperate in the localization of the golgin GCC185. Cell *132*, 286–298.

Cai, T., Fukushige, T., Notkins, A.L., and Krause, M. (2004). Insulinoma-associated protein IA-2, a vesicle transmembrane protein, genetically interacts with UNC-31/CAPS and affects neurosecretion in Caenorhabditis elegans. J. Neurosci. *24*, 3115–3124.

Callebaut, I., de Gunzburg, J., Goud, B., and Mornon, J.P. (2001). RUN domains: a new family of domains involved in Ras-like GTPase signaling. Trends Biochem. Sci. *26*, 79–83.

Cantor, R.M., Kono, N., Duvall, J.A., Alvarez-Retuerto, A., Stone, J.L., Alarcón, M., Nelson, S.F., and Geschwind, D.H. (2005). Replication of autism linkage: fine-mapping peak at 17q21. Am. J. Hum. Genet. *76*, 1050–1056.

Charlie, N.K., Schade, M.A., Thomure, A.M., and Miller, K.G. (2006). Presynaptic UNC-31 (CAPS) is required to activate the G alpha(s) pathway of the Caenorhabditis elegans synaptic signaling network. Genetics *172*, 943–961.

Chavrier, P., Parton, R.G., Hauri, H.P., Simons, K., and Zerial, M. (1990). Localization of low molecular weight GTP binding proteins to exocytic and endocytic compartments. Cell *62*, 317–329.

Chun, D.K., McEwen, J.M., Burbea, M., and Kaplan, J.M. (2008). UNC-108/Rab2 regulates postendocytic trafficking in Caenorhabditis elegans. Mol. Biol. Cell *19*, 2682–2695.

Cormont, M., Mari, M., Galmiche, A., Hofman, P., and Le Marchand-Brustel, Y. (2001). A FYVE-finger-containing protein, Rabip4, is a Rab4 effector involved in early endosomal traffic. Proc. Natl. Acad. Sci. USA *98*, 1637–1642.

Davis, M.W., Hammarlund, M., Harrach, T., Hullett, P., Olsen, S., and Jorgensen, E.M. (2005). Rapid single nucleotide polymorphism mapping in C. elegans. BMC Genomics *6*, 118.

De Stasio, E.A., and Dorman, S. (2001). Optimization of ENU mutagenesis of Caenorhabditis elegans. Mutat. Res. *495*, 81–88.

Dikeakos, J.D., and Reudelhuber, T.L. (2007). Sending proteins to dense core secretory granules: still a lot to sort out. J. Cell Biol. *177*, 191–196.

Dikeakos, J.D., Di Lello, P., Lacombe, M.-J., Ghirlando, R., Legault, P., Reudelhuber, T.L., and Omichinski, J.G. (2009). Functional and structural characterization of a dense core secretory granule sorting domain from the PC1/3 protease. Proc. Natl. Acad. Sci. USA *106*, 7408–7413.

Dittie, A.S., Hajibagheri, N., and Tooze, S.A. (1996). The AP-1 adaptor complex binds to immature secretory granules from PC12 cells, and is regulated by ADP-ribosylation factor. J. Cell Biol. *132*, 523–536.

Doi, M., and Iwasaki, K. (2002). Regulation of retrograde signaling at neuromuscular junctions by the novel C2 domain protein AEX-1. Neuron *33*, 249–259.

Edwards, S.L., Charlie, N.K., Richmond, J.E., Hegermann, J., Eimer, S., and Miller, K.G. (2009). Impaired dense core vesicle maturation in Caenorhabditis elegans mutants lacking Rab2. J. Cell Biol. *186*, 881–895.

Fouraux, M.A., Deneka, M., Ivan, V., van der Heijden, A., Raymackers, J., van Suylekom, D., van Venrooij, W.J., van der Sluijs, P., and Pruijn, G.J.M. (2004). Rabip4′ is an effector of rab5 and rab4 and regulates transport through early endosomes. Mol. Biol. Cell *15*, 611–624.

Frost, A., Unger, V.M., and De Camilli, P. (2009). The BAR domain superfamily: membrane-molding macromolecules. Cell *137*, 191–196.

Fukuda, M., Kobayashi, H., Ishibashi, K., and Ohbayashi, N. (2011). Genome-wide investigation of the Rab binding activity of RUN domains: development of a novel tool that specifically traps GTP-Rab35. Cell Struct. Funct. *36*, 155–170.

Gaglia, M.M., and Kenyon, C. (2009). Stimulation of movement in a quiescent, hibernation-like form of Caenorhabditis elegans by dopamine signaling. J. Neurosci. *29*, 7302–7314.

Goud, B., Zahraoui, A., Tavitian, A., and Saraste, J. (1990). Small GTP-binding protein associated with Golgi cisternae. Nature *345*, 553–556.

Gracheva, E.O., Burdina, A.O., Touroutine, D., Berthelot-Grosjean, M., Parekh, H., and Richmond, J.E. (2007). Tomosyn negatively regulates CAPS-dependent peptide release at Caenorhabditis elegans synapses. J. Neurosci. *27*, 10176–10184.

Grigoriev, I., Splinter, D., Keijzer, N., Wulf, P.S., Demmers, J., Ohtsuka, T., Modesti, M., Maly, I.V., Grosveld, F., Hoogenraad, C.C., and Akhmanova, A. (2007). Rab6 regulates transport and targeting of exocytotic carriers. Dev. Cell *13*, 305–314.

Hannemann, M., Sasidharan, N., Hegermann, J., Kutscher, L.M., Koenig, S., and Eimer, S. (2012). TBC-8, a putative RAB-2 GAP, regulates dense core vesicle maturation in Caenorhabditis elegans. PLoS Genet. *8*, e1002722.

Hayes, G.L., Brown, F.C., Haas, A.K., Nottingham, R.M., Barr, F.A., and Pfeffer, S.R. (2009). Multiple Rab GTPase binding sites in GCC185 suggest a model for vesicle tethering at the trans-Golgi. Mol. Biol. Cell *20*, 209–217.

Hobson, R.J., Liu, Q., Watanabe, S., and Jorgensen, E.M. (2011). Complexin maintains vesicles in the primed state in C. elegans. Curr. Biol. *21*, 106–113.

Husson, S.J., Clynen, E., Baggerman, G., Janssen, T., and Schoofs, L. (2006). Defective processing of neuropeptide precursors in Caenorhabditis elegans lacking proprotein convertase 2 (KPC-2/EGL-3): mutant analysis by mass spectrometry. J. Neurochem. *98*, 1999–2012.

Janoueix-Lerosey, I., Jollivet, F., Camonis, J., Marche, P.N., and Goud, B. (1995). Two-hybrid system screen with the small GTP-binding protein Rab6. Identification of a novel mouse GDP dissociation inhibitor isoform and two other potential partners of Rab6. J. Biol. Chem. *270*, 14801–14808.

Janoueix-Lerosey, I., Pasheva, E., de Tand, M.F., Tavitian, A., and de Gunzburg, J. (1998). Identification of a specific effector of the small GTP-binding protein Rap2. Eur. J. Biochem. *252*, 290–298.

Jockusch, W.J., Speidel, D., Sigler, A., Sørensen, J.B., Varoqueaux, F., Rhee, J.-S., and Brose, N. (2007). CAPS-1 and CAPS-2 are essential synaptic vesicle priming proteins. Cell *131*, 796–808.

Kakhlon, O., Sakya, P., Larijani, B., Watson, R., and Tooze, S.A. (2006). GGA function is required for maturation of neuroendocrine secretory granules. EMBO J. *25*, 1590–1602.

Kass, J., Jacob, T.C., Kim, P., and Kaplan, J.M. (2001). The EGL-3 proprotein convertase regulates mechanosensory responses of Caenorhabditis elegans. J. Neurosci. *21*, 9265–9272.

Kim, T., Gondré-Lewis, M.C., Arnaoutova, I., and Loh, Y.P. (2006). Dense-core secretory granule biogenesis. Physiology (Bethesda) *21*, 124–133.

Klumperman, J., Kuliawat, R., Griffith, J.M., Geuze, H.J., and Arvan, P. (1998). Mannose 6-phosphate receptors are sorted from immature secretory granules via adaptor protein AP-1, clathrin, and syntaxin 6-positive vesicles. J. Cell Biol. *141*, 359–371.

Kukimoto-Niino, M., Takagi, T., Akasaka, R., Murayama, K., Uchikubo-Kamo, T., Terada, T., Inoue, M., Watanabe, S., Tanaka, A., Hayashizaki, Y., et al. (2006). Crystal structure of the RUN domain of the RAP2-interacting protein x. J. Biol. Chem. *281*, 31843–31853.

Lan, Z., Kurata, W.E., Martyn, K.D., Jin, C., and Lau, A.F. (2005). Novel rab GAP-like protein, CIP85, interacts with connexin43 and induces its degradation. Biochemistry *44*, 2385–2396.

Leinwand, S.G., and Chalasani, S.H. (2013). Neuropeptide signaling remodels chemosensory circuit composition in Caenorhabditis elegans. Nat. Neurosci. *16*, 1461–1467.

Llanos, S., Efeyan, A., Monsech, J., Dominguez, O., and Serrano, M. (2006). A high-throughput loss-of-function screening identifies novel p53 regulators. Cell Cycle *5*, 1880–1885.

Lundquist, E.A. (2006). Small GTPases. WormBook, 1–18.

Matsunaga, K., Saitoh, T., Tabata, K., Omori, H., Satoh, T., Kurotori, N., Maejima, I., Shirahama-Noda, K., Ichimura, T., Isobe, T., et al. (2009). Two Beclin 1-binding proteins, Atg14L and Rubicon, reciprocally regulate autophagy at different stages. Nat. Cell Biol. *11*, 385–396.

McIntire, S.L., Reimer, R.J., Schuske, K., Edwards, R.H., and Jorgensen, E.M. (1997). Identification and characterization of the vesicular GABA transporter. Nature *389*, 870–876.

Miller, K.G., Emerson, M.D., and Rand, J.B. (1999). Goalpha and diacylglycerol kinase negatively regulate the Gqalpha pathway in C. elegans. Neuron *24*, 323–333.

Miserey-Lenkei, S., Waharte, F., Boulet, A., Cuif, M.-H., Tenza, D., El Marjou, A., Raposo, G., Salamero, J., Héliot, L., Goud, B., and Monier, S. (2007). Rab6-interacting protein 1 links Rab6 and Rab11 function. Traffic *8*, 1385–1403.

Mori, T., Wada, T., Suzuki, T., Kubota, Y., and Inagaki, N. (2007). Singar1, a novel RUN domain-containing protein, suppresses formation of surplus axons for neuronal polarity. J. Biol. Chem. *282*, 19884–19893.

Munro, S. (2011). The golgin coiled-coil proteins of the Golgi apparatus. Cold Spring Harb. Perspect. Biol. *3*, 3.

Park, J.J., and Loh, Y.P. (2008). How peptide hormone vesicles are transported to the secretion site for exocytosis. Mol. Endocrinol. *22*, 2583–2595.

Pereira-Leal, J.B., and Seabra, M.C. (2001). Evolution of the Rab family of small GTP-binding proteins. J. Mol. Biol. *313*, 889–901.

Pierce, S.B., Costa, M., Wisotzkey, R., Devadhar, S., Homburger, S.A., Buchman, A.R., Ferguson, K.C., Heller, J., Platt, D.M., Pasquinelli, A.A., et al. (2001). Regulation of DAF-2 receptor signaling by human insulin and ins-1, a member of the unusually large and diverse C. elegans insulin gene family. Genes Dev. *15*, 672–686.

Recacha, R., Boulet, A., Jollivet, F., Monier, S., Houdusse, A., Goud, B., and Khan, A.R. (2009). Structural basis for recruitment of Rab6-interacting protein 1 to Golgi via a RUN domain. Structure *17*, 21–30.

Sanders, S.J., Murtha, M.T., Gupta, A.R., Murdoch, J.D., Raubeson, M.J., Willsey, A.J., Ercan-Sencicek, A.G., DiLullo, N.M., Parikshak, N.N., Stein, J.L., et al. (2012). De novo mutations revealed by whole-exome sequencing are strongly associated with autism. Nature *485*, 237–241.

Shi, A., Chen, C.C.-H., Banerjee, R., Glodowski, D., Audhya, A., Rongo, C., and Grant, B.D. (2010). EHBP-1 functions with RAB-10 during endocytic recycling in Caenorhabditis elegans. Mol. Biol. Cell *21*, 2930–2943.

Short, B., Preisinger, C., Körner, R., Kopajtich, R., Byron, O., and Barr, F.A. (2001). A GRASP55-rab2 effector complex linking Golgi structure to membrane traffic. J. Cell Biol. *155*, 877–883.

Sieburth, D., Madison, J.M., and Kaplan, J.M. (2007). PKC-1 regulates secretion of neuropeptides. Nat. Neurosci. *10*, 49–57.

Singh, K., Chao, M.Y., Somers, G.A., Komatsu, H., Corkins, M.E., Larkins-Ford, J., Tucey, T., Dionne, H.M., Walsh, M.B., Beaumont, E.K., et al. (2011). C. elegans Notch signaling regulates adult chemosensory response and larval molting quiescence. Curr. Biol. *21*, 825–834.

Sinka, R., Gillingham, A.K., Kondylis, V., and Munro, S. (2008). Golgi coiled-coil proteins contain multiple binding sites for Rab family G proteins. J. Cell Biol. *183*, 607–615.

Speese, S., Petrie, M., Schuske, K., Ailion, M., Ann, K., Iwasaki, K., Jorgensen, E.M., and Martin, T.F.J. (2007). UNC-31 (CAPS) is required for dense-core vesicle but not synaptic vesicle exocytosis in Caenorhabditis elegans. J. Neurosci. *27*, 6150–6162.

Stenmark, H. (2009). Rab GTPases as coordinators of vesicle traffic. Nat. Rev. Mol. Cell Biol. *10*, 513–525.

Sumakovic, M., Hegermann, J., Luo, L., Husson, S.J., Schwarze, K., Olendrowitz, C., Schoofs, L., Richmond, J., and Eimer, S. (2009). UNC-108/RAB-2 and its effector RIC-19 are involved in dense core vesicle maturation in Caenorhabditis elegans. J. Cell Biol. *186*, 897–914.

Tisdale, E.J., Bourne, J.R., Khosravi-Far, R., Der, C.J., and Balch, W.E. (1992). GTP-binding mutants of rab1 and rab2 are potent inhibitors of vesicular transport from the endoplasmic reticulum to the Golgi complex. J. Cell Biol. *119*, 749–761.

Tooze, S.A., Flatmark, T., Tooze, J., and Huttner, W.B. (1991). Characterization of the immature secretory granule, an intermediate in granule biogenesis. J. Cell Biol. *115*, 1491–1503.

Tooze, S.A., Martens, G.J., and Huttner, W.B. (2001). Secretory granule biogenesis: rafting to the SNARE. Trends Cell Biol. *11*, 116–122.

Urbé, S., Page, L.J., and Tooze, S.A. (1998). Homotypic fusion of immature secretory granules during maturation in a cell-free assay. J. Cell Biol. *143*, 1831–1844.

Van Buskirk, C., and Sternberg, P.W. (2007). Epidermal growth factor signaling induces behavioral quiescence in Caenorhabditis elegans. Nat. Neurosci. *10*, 1300–1307.

van 't Veer, L.J., Dai, H., van de Vijver, M.J., He, Y.D., Hart, A.A.M., Mao, M., Peterse, H.L., van der Kooy, K., Marton, M.J., Witteveen, A.T., et al. (2002). Gene expression profiling predicts clinical outcome of breast cancer. Nature *415*, 530–536.

Walent, J.H., Porter, B.W., and Martin, T.F. (1992). A novel 145 kd brain cytosolic protein reconstitutes Ca(2+)-regulated secretion in permeable neuroendocrine cells. Cell *70*, 765–775.

Watanabe, S., Punge, A., Hollopeter, G., Willig, K.I., Hobson, R.J., Davis, M.W., Hell, S.W., and Jorgensen, E.M. (2011). Protein localization in electron micrographs using fluorescence nanoscopy. Nat. Methods *8*, 80–84.

Wendler, F., Page, L., Urbé, S., and Tooze, S.A. (2001). Homotypic fusion of immature secretory granules during maturation requires syntaxin 6. Mol. Biol. Cell *12*, 1699–1709.

White, J.Q., Nicholas, T.J., Gritton, J., Truong, L., Davidson, E.R., and Jorgensen, E.M. (2007). The sensory circuitry for sexual attraction in C. elegans males. Curr. Biol. *17*, 1847–1857.

Yang, J., Kim, O., Wu, J., and Qiu, Y. (2002). Interaction between tyrosine kinase Etk and a RUN domain- and FYVE domain-containing protein RUFY1. A possible role of ETK in regulation of vesicle trafficking. J. Biol. Chem. *277*, 30219–30226.

You, Y.J., Kim, J., Raizen, D.M., and Avery, L. (2008). Insulin, cGMP, and TGF-beta signals regulate food intake and quiescence in C. elegans: a model for satiety. Cell Metab. *7*, 249–257.

Yu, I.-M., and Hughson, F.M. (2010). Tethering factors as organizers of intracellular vesicular traffic. Annu. Rev. Cell Dev. Biol. *26*, 137–156.

Zerial, M., and McBride, H. (2001). Rab proteins as membrane organizers. Nat. Rev. Mol. Cell Biol. *2*, 107–117.

Zhong, Y., Wang, Q.J., Li, X., Yan, Y., Backer, J.M., Chait, B.T., Heintz, N., and Yue, Z. (2009). Distinct regulation of autophagic activity by Atg14L and Rubicon associated with Beclin 1-phosphatidylinositol-3-kinase complex. Nat. Cell Biol. *11*, 468–476.

Zhou, K.-M., Dong, Y.-M., Ge, Q., Zhu, D., Zhou, W., Lin, X.-G., Liang, T., Wu, Z.-X., and Xu, T. (2007). PKA activation bypasses the requirement for UNC-31 in the docking of dense core vesicles from C. elegans neurons. Neuron *56*, 657–669.

Neuron, Volume *82*

Supplemental Information

Two Rab2 Interactors Regulate Dense-Core Vesicle Maturation

Michael Ailion, Mandy Hannemann, Susan Dalton, Andrea Pappas, Shigeki Watanabe, Jan Hegermann, Qiang Liu, Hsiao-Fen Han, Mingyu Gu, Morgan Q. Goulding, Nikhil Sasidharan, Kim Schuske, Patrick Hullett, Stefan Eimer, and Erik M. Jorgensen

RUND-1 alignment

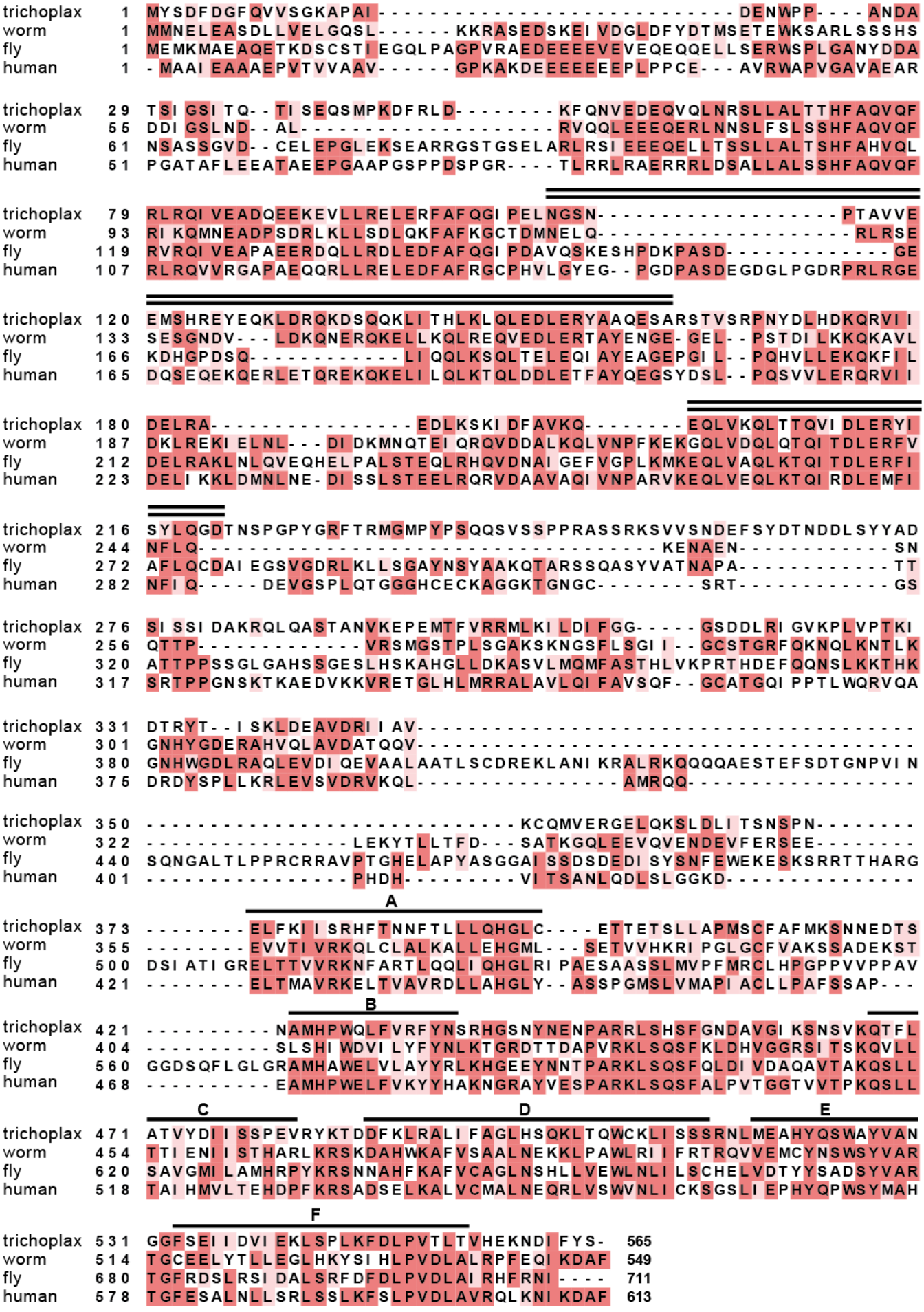

CCCP-1 alignment

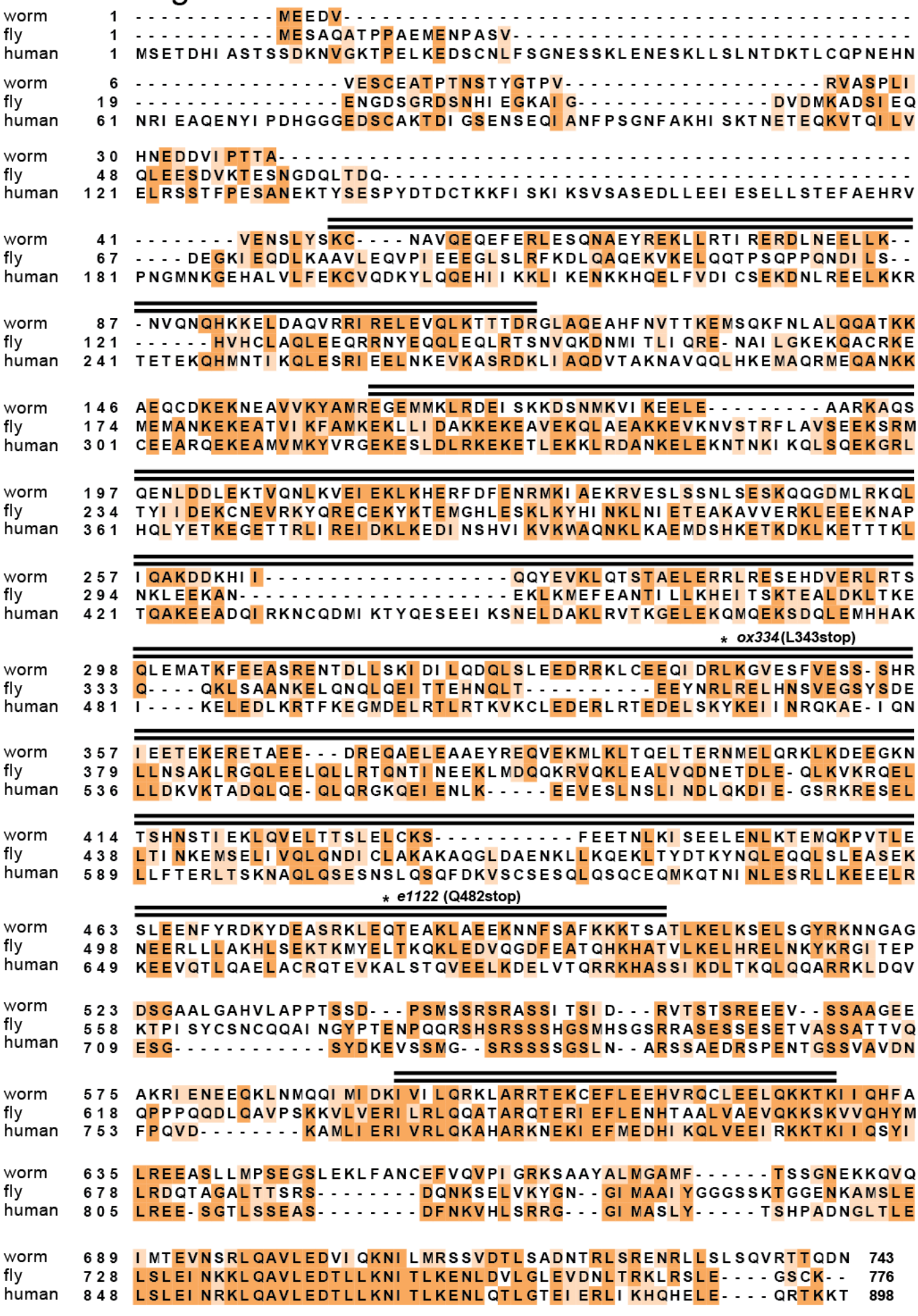

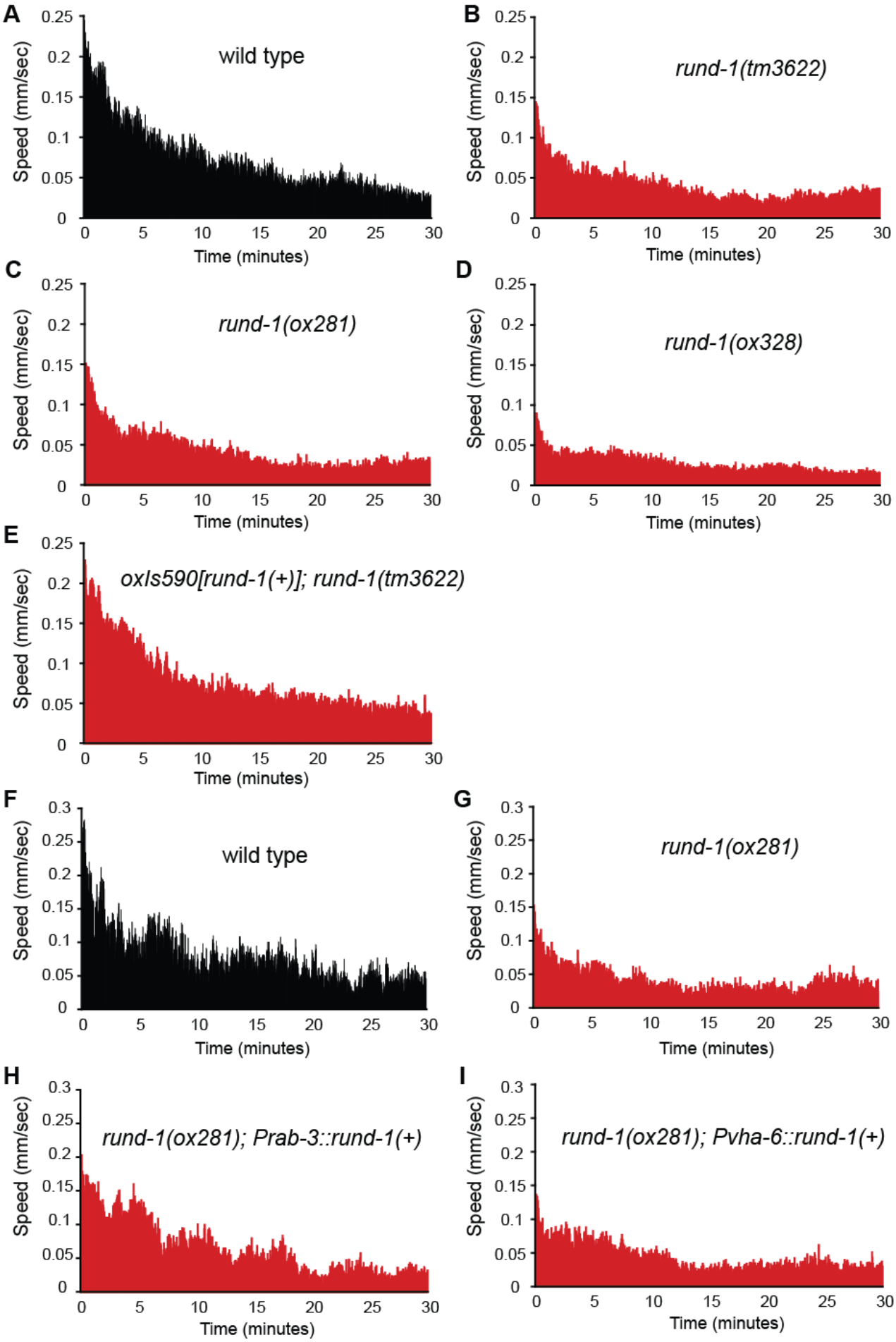
A
wild type
B
rund-1(tm3622)
C
rund-1(ox281)
D
rund-1(ox328)
E
oxIs590[rund-1(+)]; rund-1(tm3622)
F
wild type
G
rund-1(ox281)
H
rund-1(ox281); Prab-3::rund-1(+)
I
rund-1(ox281); Pvha-6::rund-1(+)
Speed (mm/sec)
Time (minutes)

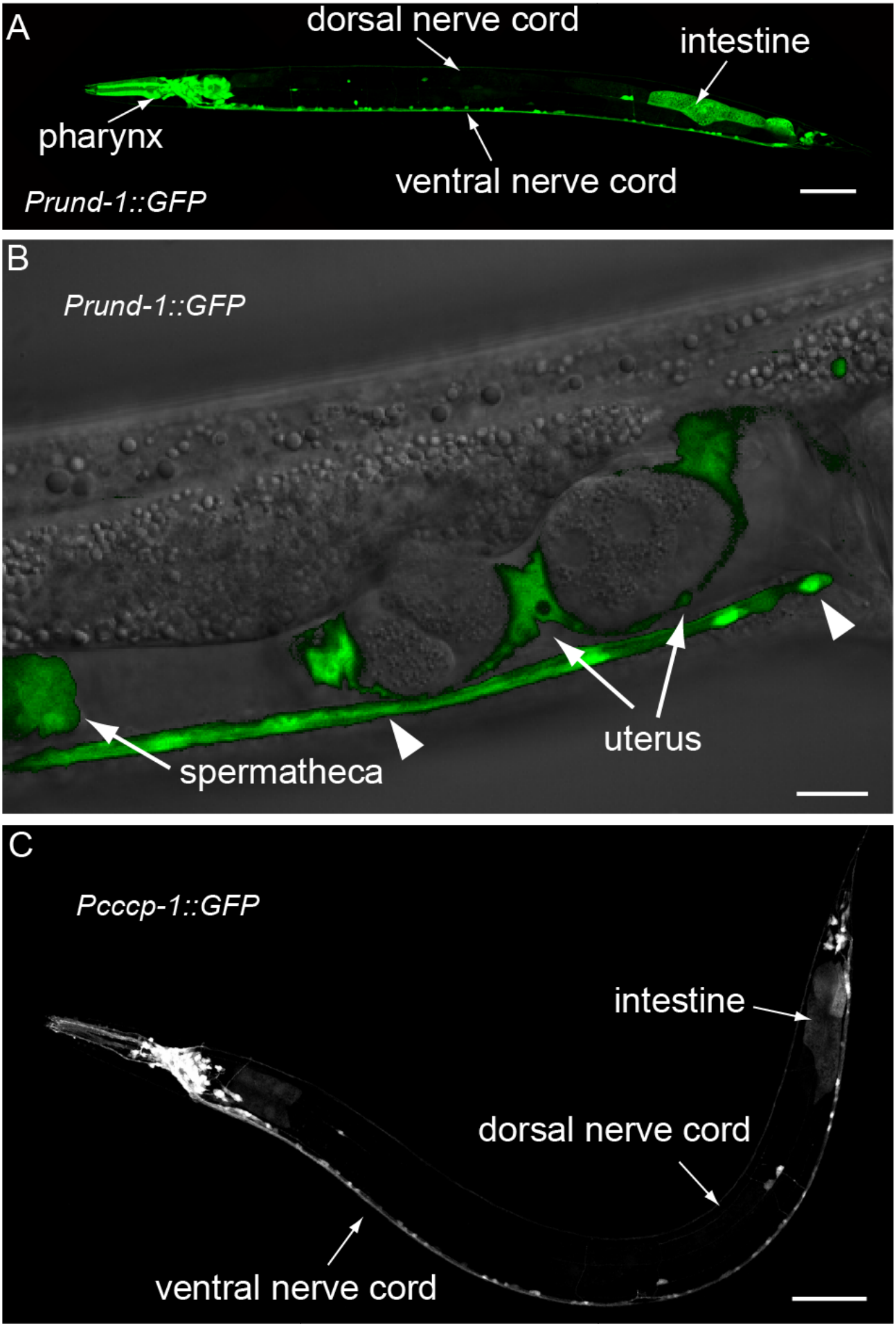
A
dorsal nerve cord
intestine
pharynx
ventral nerve cord
Prund-1::GFP
B
Prund-1::GFP
uterus
spermatheca
C
Pcccp-1::GFP
intestine
dorsal nerve cord
ventral nerve cord

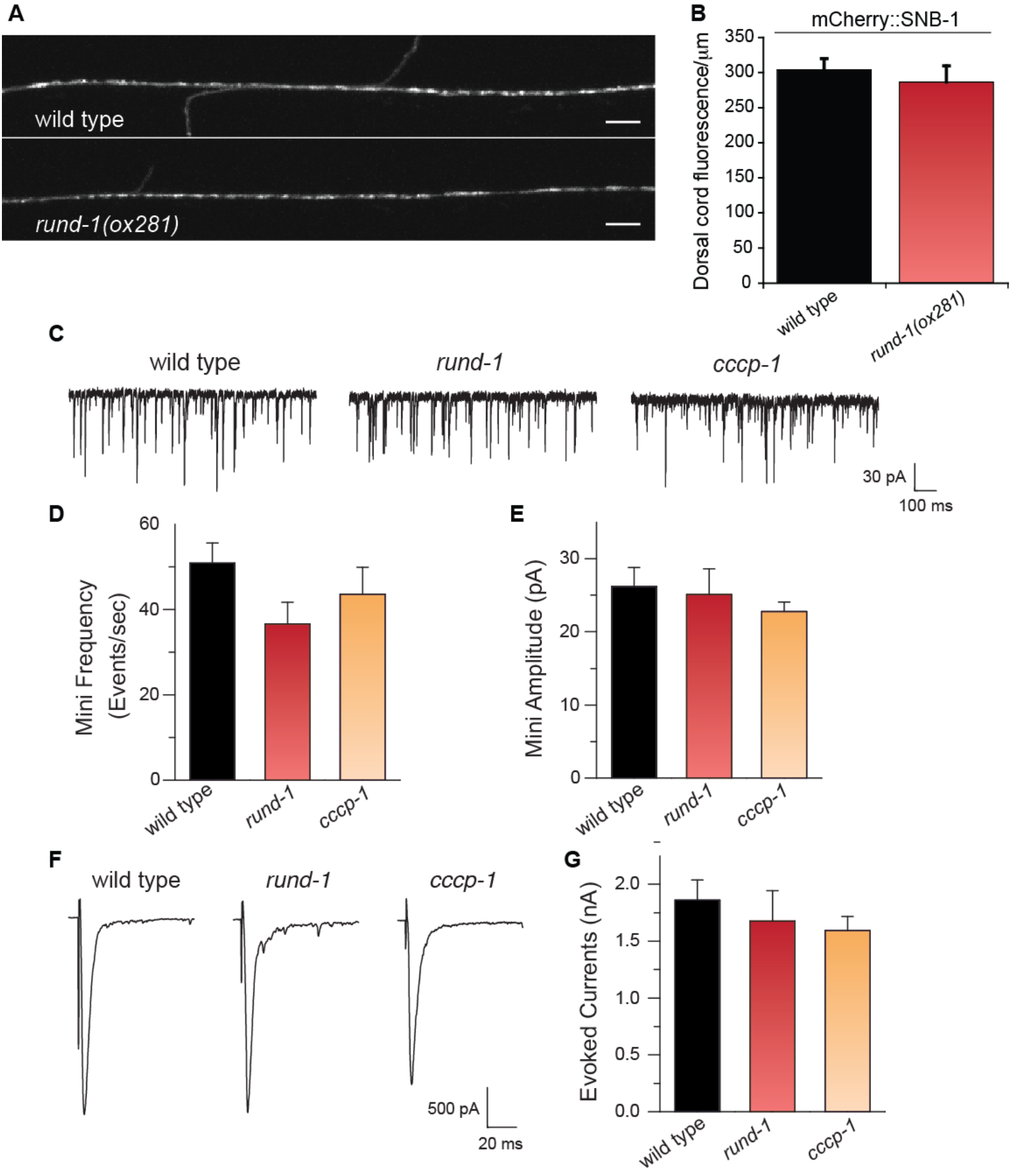
A
wild type
rund-1(ox281)
B
mCherry::SNB-1
Dorsal cord fluorescence/µm
350
300
250
200
150
100
50
0
wild type
rund-1(ox281)
C
wild type
rund-1
cccp-1
30 pA
100 ms
D
Mini Frequency (Events/sec)
60
40
20
0
wild type
rund-1
cccp-1
E
Mini Amplitude (pA)
30
20
10
0
wild type
rund-1
cccp-1
F
wild type
rund-1
cccp-1
500 pA
20 ms
G
Evoked Currents (nA)
2.0
1.5
1.0
0.5
0.0
wild type
rund-1
cccp-1

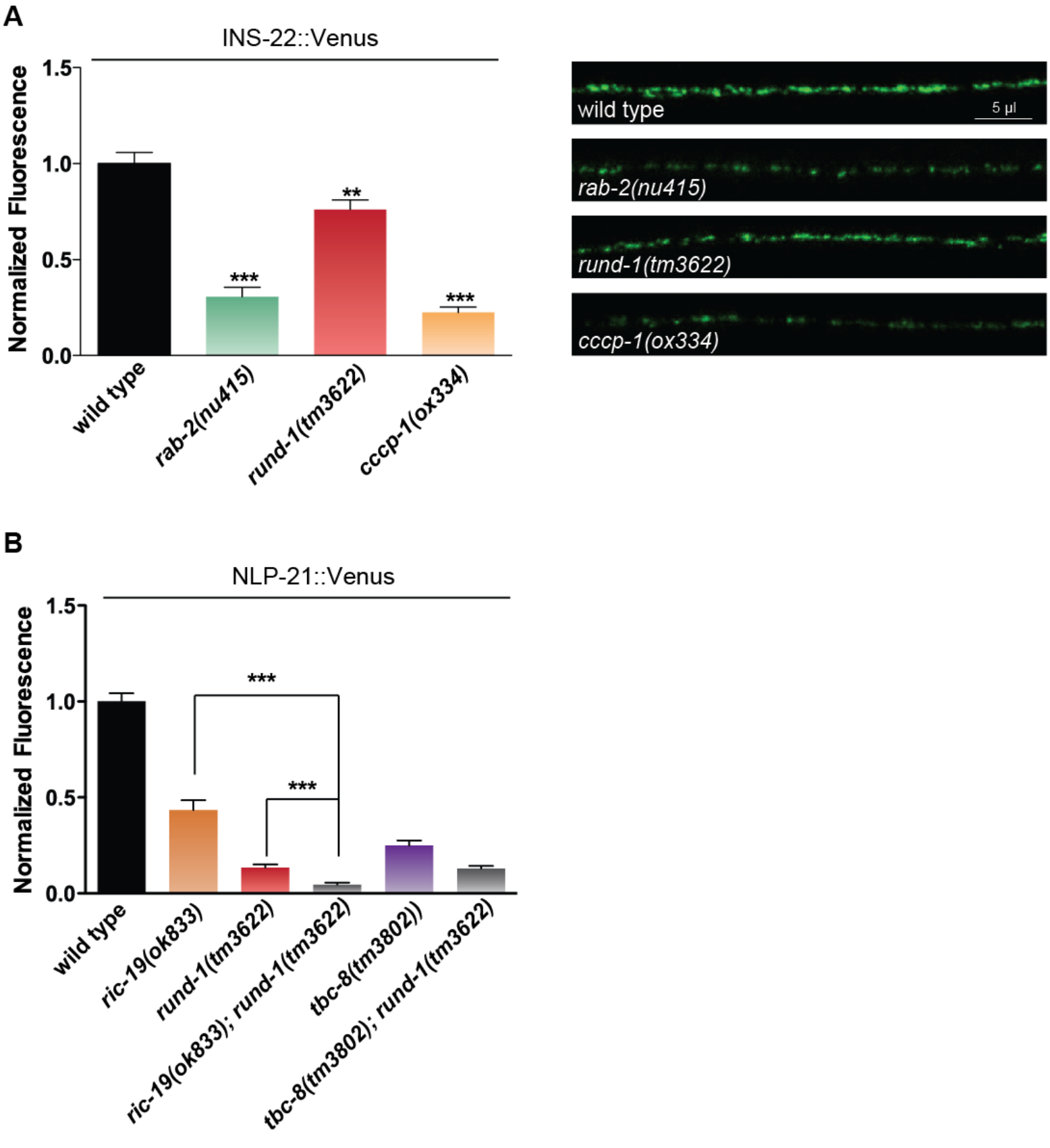
A
INS-22::Venus
Normalized Fluorescence
1.5
1.0
0.5
0.0
**
***
***
wild type
rab-2(nu415)
rund-1(tm3622)
cccp-1(ox334)
wild type
5 µl
rab-2(nu415)
rund-1(tm3622)
cccp-1(ox334)
B
NLP-21::Venus
Normalized Fluorescence
1.5
1.0
0.5
0.0
***
***
wild type
ric-19(ok833)
rund-1(tm3622)
ric-19(ok833); rund-1(tm3622)
tbc-8(tm3802))
tbc-8(tm3802); rund-1(tm3622)

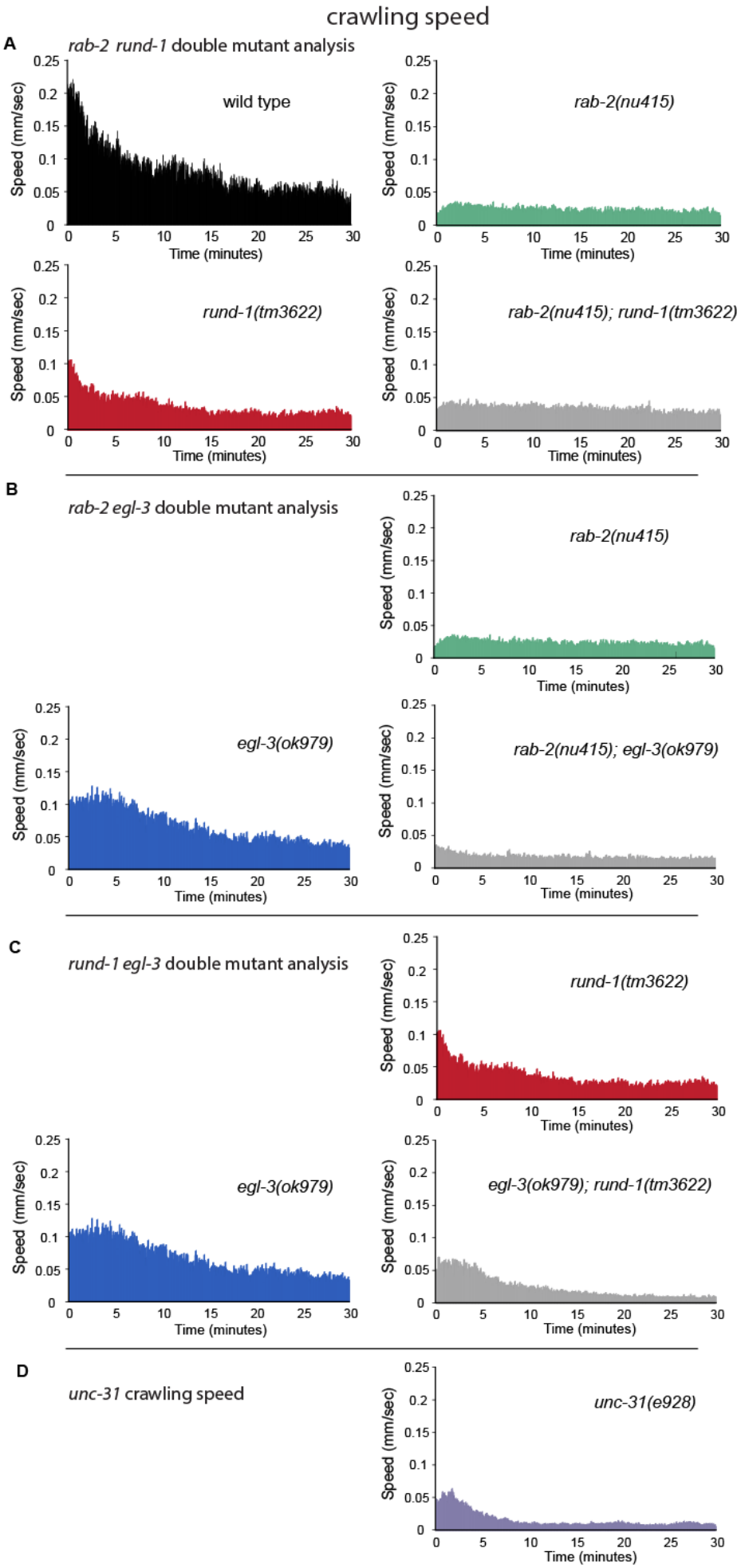
crawling speed
A
rab-2 rund-1 double mutant analysis
wild type
rab-2(nu415)
rund-1(tm3622)
rab-2(nu415); rund-1(tm3622)
B
rab-2 egl-3 double mutant analysis
rab-2(nu415)
egl-3(ok979)
rab-2(nu415); egl-3(ok979)
C
rund-1 egl-3 double mutant analysis
rund-1(tm3622)
egl-3(ok979)
egl-3(ok979); rund-1(tm3622)
D
unc-31 crawling speed
unc-31(e928)
Speed (mm/sec)
Time (minutes)
0
0.05
0.1
0.15
0.2
0.25
0
5
10
15
20
25
30

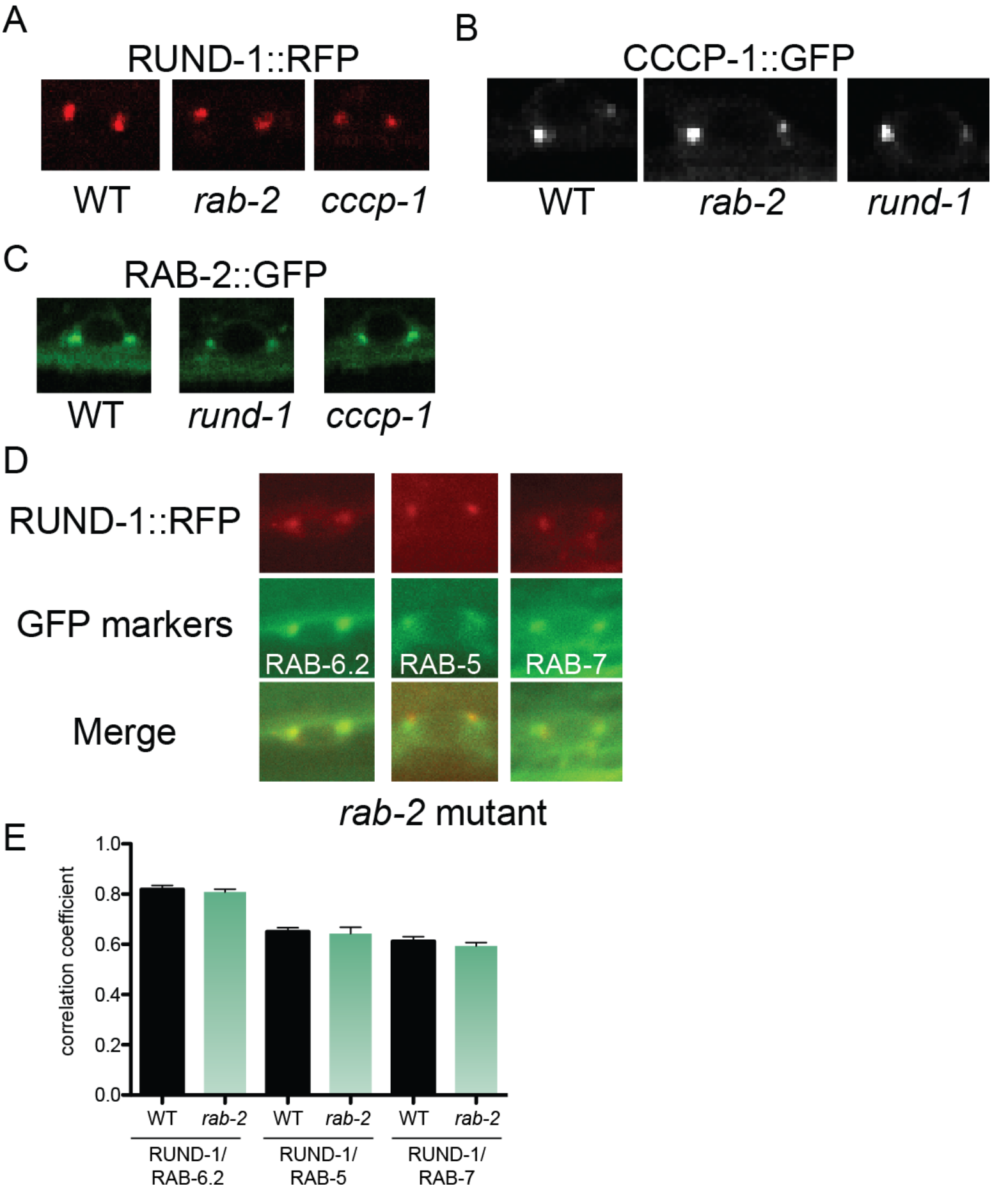
A
RUND-1::RFP
WT
rab-2
cccp-1
B
CCCP-1::GFP
WT
rab-2
rund-1
C
RAB-2::GFP
WT
rund-1
cccp-1
D
RUND-1::RFP
GFP markers
Merge
RAB-6.2
RAB-5
RAB-7
rab-2 mutant
E
correlation coefficient
1.0
0.8
0.6
0.4
0.2
0.0
WT
rab-2
WT
rab-2
WT
rab-2
RUND-1/ RAB-6.2
RUND-1/ RAB-5
RUND-1/ RAB-7

Supplemental Information

Supplemental Figure and Movie Legends

Figure S1. Alignment of the full-length RUND-1 protein. (related to Figure 1)
Alignment of *C. elegans* RUND-1 (worm, accession # JN986879) and its orthologs from *Trichoplax adhaerens* (Trichoplax, hypothetical protein TRIADDRAFT_52054, accession # XP_002108010.1), *Drosophila melanogaster* (fly, CG3703, accession # NP_569874.1) and *Homo sapiens* (human, RUNDC1, accession # AAH39247.1). Identical residues are shaded in darker red and similar residues are shaded in lighter red. The coiled-coil domains (from SMART, using the worm protein; http://smart.embl-heidelberg.de/) are marked with double black bars. The six conserved blocks A-F of the RUN domain (Callebaut et al., 2001) are marked with single black bars. Alignment was made with MUSCLE (Edgar, 2004) using default parameters and exhibited with Boxshade 3.21 (http://www.ch.embnet.org/software/BOX_form.html).

Figure S2. Alignment of the full-length CCCP-1b protein. (related to Figure 1)
Alignment of *C. elegans* CCCP-1b (worm, accession # JN986880) and its orthologs from *Drosophila melanogaster* (fly, CG4925, accession # NP_648879.1) and *Homo sapiens* (human, C10orf118, accession # AAI03500.1). Identical residues are shaded in darker yellow and similar residues are shaded in lighter yellow. The coiled-coil domains (from SMART, using the worm protein; http://smart.embl-heidelberg.de/) are marked with double black bars. The positions of the *ox334* and *e1122* stop mutations are marked with asterisks. Alignment was made with MUSCLE (Edgar, 2004) using default parameters and exhibited with Boxshade 3.21 (http://www.ch.embnet.org/software/BOX_form.html).

Figure S3. Locomotion data. (related to Figure 2)
(A-E) Each graph shows the mean speed of 21 to 27 animals during the 30 minute period immediately after being transferred to a new plate. These graphs show the complete tracking data associated with the left side of Figure 2C.
(F-I) Each graph shows the mean speed of 9 animals during the 30 minute period immediately after being transferred to a new plate. These graphs show the complete tracking data associated with the right side of Figure 2C.

Figure S4. *rund-1* and *cccp-1* are expressed widely in neurons and other tissues.
Expression of *rund-1* and *cccp-1* promoter::GFP fusions are shown in transgenic animals carrying extrachromosomal arrays.
(A) An L4 stage late-larval animal is shown. *Prund-1::GFP* is expressed throughout the nervous system, including head and tail neurons and motor neurons in the ventral cord. Expression is also observed in the pharynx and intestine, but not in skin or muscle cells. This animal has intestinal expression in only the posterior intestine due to mosaicism of the extrachromosomal array. Scale bar: 50 μm.
(B) Expression of *Prund-1::GFP* in the spermatheca, uterus and ventral nerve cord (arrowheads) of a gravid adult. GFP and DIC images are superimposed. Scale bar: 10 μm.
(C) An L4 stage late-larval animal is shown. *Pcccp-1::GFP* is expressed throughout the nervous system, including head and tail neurons and motor neurons in the ventral cord. Expression is also seen in the intestine, but is not seen in pharynx, skin or muscle cells. This animal has intestinal expression in only the posterior intestine due to mosaicism of the extrachromosomal array. Scale bar: 50 μm.

Figure S5. *rund-1* and *cccp-1* mutants do not have defects in development or function of synapses.
(A) *rund-1(ox281)* shows normal synaptic development as visualized by *Punc-129::mCherry::snb-1* localization in the dorsal nerve cord of young adult animals. Scale bar: 5 μm.
(B) Quantification of mCherry::SNB-1 fluorescence levels in the dorsal cord. The mean fluorescence intensity per μm is given in arbitrary units. The *rund-1(ox281)* mutant has normal levels of mCherry::SNB-1 in the dorsal cord (P=0.55, two-tailed unpaired t test). Error bars = SEM; n = 6 animals each genotype.
(C) Representative traces of endogenous currents (minis) in wild-type, *rund-1(tm3622)* and *cccp-1(ox334)*.
(D,E) *rund-1* and *cccp-1* mutants have normal mini frequency and amplitude (P>0.05, paired t test). Error bars = SEM; n = 8 animals each genotype.
(F) Representative traces of electrically evoked currents in wild-type, *rund-1(tm3622)* and *cccp-1(ox334)*.
(G) *rund-1* and *cccp-1* mutants have normal evoked currents (P>0.05, paired t test). Error bars = SEM; n = 6-8 animals each genotype.

Figure S6. Dense-core vesicle trafficking phenotypes.
(A) The graph shows quantification of INS-22::Venus fluorescence levels in the dorsal nerve cord. The images show representative examples of the data. *rab-2*, *rund-1*, and *cccp-1* mutants all have decreased trafficking of INS-22::Venus to the dorsal nerve cord (***, P<0.001 compared to wild type; **, P<0.01). Error bars = SEM; n = 18-21 animals each genotype.
(B) *rund-1* and *ric-19* act in parallel. The graph shows quantification of NLP-21::Venus fluorescence levels in the dorsal nerve cord. A *ric-19; rund-1* double mutant has a stronger defect than either a *ric-19* or *rund-1* single mutant (***, P<0.001 for both comparisons). A *tbc-8; rund-1* double mutant does not have a stronger defect than the *rund-1* single mutant (P>0.05). Error bars = SEM; n = 14-70 animals each genotype.

Figure S7. Locomotion data. (related to Figure 2)
Each graph shows the mean speed of 24 to 31 animals during a 30 minute period immediately after being transferred to a new plate. The graphs in panel A show the complete tracking data associated with Figure 2E. Graphs of *rab-2*, *rund-1*, and *egl-3* are repeated in panels A-C for ease of comparison. Though *rab-2* mutants are similar to *rund-1* and *cccp-1* mutants at steady state, *rab-2* mutants are not stimulated by harsh touch like *rund-1*, *cccp-1*, and even *unc-31*/CAPS mutants. The additional lack of stimulated locomotion in *rab-2* mutants may be due to a RAB-2 function that does not require CAPS and thus is likely to be unrelated to dense-core vesicle function.

Figure S8. RUND-1, RAB-2 and CCCP-1 are not required for each other's localization (related to Figure 5)
Each panel shows a single slice of a confocal (A-C) or wide-field (D) image of motor neuron cell bodies in the ventral nerve cord of young adult animals.
(A) RUND-1::RFP is still localized in *rab-2(nu415)* and *cccp-1(ox334)* mutants. The figure shows the expression of the single-copy transgene *oxIs590*.
(B) CCCP-1::GFP is still localized in *rab-2(nu415)* and *rund-1(tm3622)* mutants. The figure shows the expression of the extrachromosomal array *oxEx1366[Pcccp-1::cccp-1(+) cDNA::GFP]*.
(C) GFP::RAB-2 is still localized in *rund-1(tm3622)* and *cccp-1(ox334)* mutants. The figure shows the expression of the single-copy transgene *oxSi314*. GFP is concentrated in puncta in the cell body, but is also seen more diffusely throughout the cell body and the axons.
(D) In a *rab-2(nu415)* mutant, RUND-1::RFP still tightly colocalizes with RAB-6.2, but not with RAB-5 or RAB-7.
(E) RUND-1::RFP tightly colocalizes with RAB-6.2, but not with RAB-5 or RAB-7. The graph shows quantification of colocalization data using the Pearson's correlation coefficient. RUND-1 is

significantly more colocalized with RAB-6.2 than with RAB-5 or RAB-7 ($P<0.0001$, two-tailed unpaired t tests), but no changes in colocalization are seen in a *rab-2* mutant ($P>0.1$ for all three comparisons). Error bars = SEM; n = 10-18 cells each genotype.

Movie S1. Locomotion of the wild-type strain N2, showing normal sinusoidal movement.

Movie S2. Locomotion of the activated Gq mutant *egl-30(tg26)*. *egl-30(tg26)* mutant worms are smaller than wild-type and have hyperactive locomotion with deeper body bends and more frequent reversals.

Movie S3. *rund-1* mutants have unmotivated spontaneous locomotion but respond to touch.
The movie shows a field of *rund-1(ox328)* mutant larval and adult animals on a bacterial lawn. The worms show normal foraging behavior, but little spontaneous locomotion. Beginning at ten seconds into the video, several worms are prodded with a platinum wire worm pick. After being touched, the stimulated worms move away, exhibiting slow but coordinated locomotion.

Movie S4. *rund-1* mutants are stimulated by UV light.
The movie shows a close-up of a single *rund-1(ox328)* adult on a bacterial lawn. It exhibits normal foraging and feeding behavior, but little spontaneous locomotion. At four seconds into the video, UV light is turned on. After a few seconds delay, the worm stops feeding and moves away, exhibiting coordinated locomotion.

Supplemental Tables

Table S1. Rescue of *rund-1* mutants by the human ortholog RUNDC1.

Strain genotype	Animals picked	Presence of array	
		+	-
rund-1(ox281); P*rund-1*::RUNDC1(+)::tagRFP	Unc	0	10
	Non-Unc	10	1
rund-1(tm3622); P*rund-1*::RUNDC1(+)::tagRFP	Unc	1	9
	Non-Unc	11	0

To examine rescue of *rund-1* mutant locomotion by transgenic expression of its human ortholog RUNDC1, approximately ten putative Unc (non-rescued) and Non-Unc (rescued) adult animals were selected from a plate of each strain under a dissecting microscope and subsequently examined for the presence of the extrachromosomal array as scored by fluorescence. The experimenter was blind to the presence of the array at the time the animals were picked. There is strong correlation of the locomotion phenotype to the presence of the array in both strains, indicating that they are rescued (Fisher's Exact Test, two-tailed P value, $P<0.0001$ for both strains).

Table S2. Statistics for locomotion tracking data. (related to Figure 2)

Comparison	Test	P value
N2 vs. *rund-1(tm3622)*	Kruskal-Wallis/Dunn	<0.001
N2 vs. *rund-1(ox281)*	Kruskal-Wallis/Dunn	<0.001
N2 vs. *rund-1(ox328)*	Kruskal-Wallis/Dunn	<0.001
N2 vs. *oxIs590[rund-1(+)]; rund-1(tm3622)*	Kruskal-Wallis/Dunn	>0.05
rund-1(tm3622) vs. *rund-1(ox281)*	Kruskal-Wallis/Dunn	>0.05
rund-1(tm3622) vs. *rund-1(ox328)*	Kruskal-Wallis/Dunn	>0.05
rund-1(tm3622) vs. *oxIs590[rund-1(+)]; rund-1(tm3622)*	Kruskal-Wallis/Dunn	<0.001
rund-1(ox281) vs. *rund-1(ox328)*	Kruskal-Wallis/Dunn	<0.01
N2 vs. *rund-1(ox281); oxEx1197 [Prab-3::rund-1(+)]*	One-way ANOVA/Bonferroni	<0.05
rund-1(ox281) vs. *rund-1(ox281); oxEx1197 [Prab-3::rund-1(+)]*	One-way ANOVA/Bonferroni	<0.01
rund-1(ox281) vs. *rund-1(ox281); oxEx1260 [Pvha-6::rund-1(+)]*	One-way ANOVA/Bonferroni	>0.05
rab-2(nu415) vs. *rund-1(tm3622)*	One-way ANOVA/Bonferroni Kruskal-Wallis/Dunn	<0.001 <0.001
rab-2(nu415) vs. *rab-2(nu415); rund-1(tm3622)*	One-way ANOVA/Bonferroni Kruskal-Wallis/Dunn	>0.05 >0.05
rab-2(nu415) vs. *unc-31(e928)*	One-way ANOVA/Bonferroni Kruskal-Wallis/Dunn	<0.001 <0.01
rab-2(nu415) vs. *egl-3(ok979); rab-2(nu415)*	One-way ANOVA/Bonferroni Kruskal-Wallis/Dunn	>0.05 >0.05
rund-1(tm3622) vs. *rab-2(nu415); rund-1(tm3622)*	One-way ANOVA/Bonferroni Kruskal-Wallis/Dunn	<0.001 <0.001
rund-1(tm3622) vs. *egl-3(ok979); rund-1(tm3622)*	One-way ANOVA/Bonferroni Kruskal-Wallis/Dunn	<0.001 >0.05
egl-3(ok979) vs. *unc-31(e928)*	One-way ANOVA/Bonferroni Kruskal-Wallis/Dunn	<0.001 <0.001
egl-3(ok979) vs. *egl-3(ok979); rab-2(nu415)*	One-way ANOVA/Bonferroni Kruskal-Wallis/Dunn	<0.001 <0.001
egl-3(ok979) vs. *egl-3(ok979); rund-1(tm3622)*	One-way ANOVA/Bonferroni Kruskal-Wallis/Dunn	<0.001 <0.01
unc-31(e928) vs. *egl-3(ok979); rab-2(nu415)*	One-way ANOVA/Bonferroni Kruskal-Wallis/Dunn	<0.001 <0.01
unc-31(e928) vs. *egl-3(ok979); rund-1(tm3622)*	One-way ANOVA/Bonferroni Kruskal-Wallis/Dunn	>0.05 >0.05
egl-3(ok979); rab-2(nu415) vs. *egl-3(ok979); rund-1(tm3622)*	One-way ANOVA/Bonferroni Kruskal-Wallis/Dunn	<0.001 <0.001

Extended Experimental Procedures

Analysis of *rund-1* and *cccp-1* cDNAs

We obtained the *rund-1* cDNA from the ORFeome library, and three predicted full-length SL1 trans-spliced *rund-1* cDNAs from Yuji Kohara. Restriction digests and partial sequencing indicated that all four cDNAs had the same splicing pattern (Figure 1A), with several differences from the gene structure predicted on Wormbase (exon 6 was 174 bp shorter than predicted on Wormbase, and Wormbase exon 7 was not present). The cDNAs yk772b6, yk814f3 and the ORFeome cDNA contained mutations. yk471g7 was sequenced completely and shown to be mutation free. This cDNA was cloned into a Gateway entry vector and used for rescue experiments.

We obtained three *cccp-1* cDNAs from Yuji Kohara. Sequencing revealed two alternatively spliced transcripts, *cccp-1a* (yk812f4) and *cccp-1b* (yk1517a6 and yk530g8), differing in the inclusion of exon 12 (Figure 1A). The existence of both isoforms is supported by additional EST sequences on Wormbase. *cccp-1* is trans-spliced to SL1. cDNAs yk812f4 and yk1517a6 contained mutations. yk530g8 was mutation-free and cloned into a Gateway entry vector for rescue experiments. The full-length sequences of the *rund-1* and *cccp-1b* transcripts were deposited in GenBank under accession numbers JN986879 and JN986880.

Transgenes

A complete list of constructs, including sizes of promoter regions, is provided below. Most of the constructs were made using the three slot multisite Gateway system (Invitrogen). Typically, a promoter, a coding sequence (genomic DNA or cDNA), and an N- or C-terminal fluorescent tag (eGFP or tagRFP-T) were cloned along with a 3'UTR into either pCFJ150 or pCFJ201, destination vectors used for Mos1-mediated single copy insertion (MosSCI) on chromosome II at *ttTi5605* and chromosome IV at *cxTi10882*, respectively (Frøkjaer-Jensen et al., 2008). All insertions were made by the direct injection MosSCI method. For most constructs, we isolated multiple independent insertions that behaved similarly. Extrachromosomal arrays were made by standard transformation methods (Mello et al., 1991).

Yeast two-hybrid assays

The Matchmaker yeast two-hybrid assay was performed according to the manufacturer's protocol (Clontech). *C. elegans rab*, *rap*, *ras*, and *ral* gene cDNAs were cloned into the bait vector pGBKT7, and the *rund-1* and *cccp-1b* cDNAs were cloned into the prey vector pGADT7. The appropriate plasmid combinations were transformed into the yeast strain AH109 and spread onto growth media lacking leucine and tryptophan for plasmid selection. Protein interactions were tested as follows: several clones of transformants were mixed, diluted to an OD_{600} of 0.2 and spotted onto selective plates lacking leucine, tryptophan and histidine. Interactions were identified by growth after three days. All interacting proteins were tested for self-activation by transforming the interacting plasmid with the appropriate empty vector pGBKT7 or pGADT7. Both RUND-1 and RIC-19 self-activated when expressed in the DNA binding domain vector pGBKT7 and thus could not be tested against each other.

Coimmunoprecipitation and immunoblotting

HEK293 cells were grown in high glucose (4.5 g/l) DMEM supplemented with 10% FBS, 110 mg/l sodium pyruvate, 2 mM glutamine, 100 U/ml penicillin, and 10 µg/ml streptomycin in a 5% CO_2 incubator at 37°C.

For coimmunoprecipitation, $4x10^6$ HEK293 cells were plated onto two 10 cm petri dishes. Twenty-four hours later, cells were cotransfected with V5 tagged-RUND-1 and either GFP, GFP::RIC-19 or GFP::TBC-8 using TurboFect *in vitro* Transfection Reagent according to the manufacturer's protocol (Fermentas). After 24 hours, cells were washed with PBS and harvested in lysis buffer (50

mM Tris pH 7.5, 150 mM NaCl, 1% Triton X100, 0.5 mM EDTA, 10% glycerol, Complete Mini Protease inhibitor (Roche)) for 30 min at 4°C. Lysates were pre-cleared by centrifugation at 4°C and the supernatant was incubated with 2 µg monoclonal anti-GFP antibody (clone 3E6, Invitrogen) for three hours at 4°C. Protein G Plus-sepharose beads (Pierce) were added. After incubating for two hours, the beads were washed three times with washing buffer (50 mM Tris pH 7.5, 500 mM NaCl, 0.1% Triton X100, 0.5 mM EDTA, 10% glycerol, Complete Mini Protease inhibitor (Roche)) and resuspended in Laemmli loading buffer. Samples were resolved on 10% SDS-polyacrylamide gels and blotted onto a nitrocellulose membrane. To detect coprecipitated proteins, we added a mixture of two mouse monoclonal anti-GFP antibodies (1:1000, clones 7.1 and 13.1, Roche) and monoclonal anti-V5 antibody (1:5000, Invitrogen) followed by goat anti-mouse horseradish peroxidase-conjugated secondary antibody (1:10,000, Jackson Laboratory). A FujiFilm LAS 3000 processor was used to develop images, which were then edited using ImageJ software (National Institutes of Health).

Fluorescence electron microscopy (fEM)

Correlative fEM was performed as previously described (Watanabe et al., 2011) with a slight modification in the protocol. In brief, transgenic animals expressing tdEos were high-pressure frozen and freeze-substituted in 0.1% potassium permanganate (EMS) + 0.001% osmium tetroxide (EMS) in 95% acetone (EMS). The freeze-substitution protocol was as follows: -90ºC for 30 hours, 5ºC/hour to -50ºC, -50ºC for 2 hours, and 5ºC/hour to -30ºC. The fixatives were removed at -50ºC, and a solution containing 0.1% uranyl acetate (Polysciences) was added to the specimens. The uranyl acetate solution was removed when the temperature reached -30ºC. The animals were then embedded into GMA plastic (SPI). Eighty nm thick sections were sliced and mounted onto a pre-cleaned coverglass. The PALM imaging was performed using the Zeiss PAL-M (Zeiss, Prototype Serial No. 2701000005) following the application of gold fiduciary markers (100nm; microspheres-nanospheres.com). The same sections were imaged using a backscatter electron detector on scanning electron microscope (FEI Nova Nano). The PALM and electron micrographs were aligned based on the fiduciary markers in Photoshop (Adobe Photoshop CS5). For the purpose of presentation, we applied a gradient transparency to the PALM image - only the background black pixels are transparent.

Electron microscopy of synaptic and dense-core vesicles

High pressure freeze electron microscopy and analysis of synaptic profiles were performed as described (Rostaing et al., 2004; Sumakovic et al., 2009).

Electrophysiology

Young adult hermaphrodites were used for electrophysiological analysis as described (Liu et al., 2009). In brief, animals were immobilized on a Sylgard-coated glass coverslip by applying a cyanoacrylate adhesive along the dorsal side. A longitudinal incision was made in the dorsolateral region. The cuticle flap was folded back and glued to the coverslip, exposing the ventral nerve cord and two adjacent muscle quadrants. An upright microscope (Axioskop; Carl Zeiss, Inc.) equipped with a 40x water immersion lens and 15x eyepieces was used for viewing the preparation. All experiments were performed with the bath at room temperature using single electrode (borosilicate glass, R ~ 5 MΩ) voltage clamp (Heka, EPC-10) with two stage capacitive compensation optimized at rest, and series resistance compensated to 50%. Electrically evoked responses were elicited using an electrode with a tip resistance of approximately 3–5 MΩ positioned along the ventral nerve cord approximately one muscle cell body away from the patched muscle. A square wave depolarizing current of 0.5 ms at 25 V was delivered from an SIU5 stimulation isolation unit driven by an S48 stimulator (Grass Technologies). The standard pipette solution was (all concentrations in mM) [KCl 120; KOH 20; $MgCl_2$ 4; TES 5; $CaCl_2$ 0.25; EGTA 5; Na_2ATP 4; sucrose 36] and the standard extracellular solution was [NaCl 150; KCl 5; $CaCl_2$ 5; $MgCl_2$ 1; sucrose 5; HEPES 15; glucose 10]. Experiments were controlled using PatchMaster software (Heka). Analog data were digitized at 10 kHz and filtered at 2 kHz.

List of strains

CB4856 Hawaiian wild-isolate
EG281 *rund-1(ox281) X*
EG328 *rund-1(ox328) X*
EG334 *cccp-1(ox334) III*
EG1285 *oxIs12[Punc-47:GFP, lin-15+] X lin-15(n765ts) X*
EG3404 *unc-31(e928) IV*
EG3654 *egl-30(tg26) I ; cccp-1(ox334) III*
EG3738 *gsa-1(ce81) I ; unc-31(e928) IV*
EG3741 *rund-1(ox281) X dpy-3(e27) X*
EG3765 *egl-30(tg26) I ; rund-1(ox281) X*
EG3773 *egl-30(tg26) I ; unc-2(e55) X*
EG3774 *egl-30(tg26) I ; unc-18(md299) X*
EG3775 *egl-30(tg26) I ; unc-68(e540) V*
EG3782 *egl-30(tg26) I ; egl-3(ok979) V*
EG3797 *egl-30(tg26) I ; rund-1(ox328) X*
EG4033 *egl-30(tg26) I ; unc-104(e1265) II*
EG4044 *egl-30(tg26) I ; unc-68(r1162) V*
EG4045 *unc-31(e928) IV ; rund-1(ox281) X*
EG4167 *rund-1(ox281) X ; oxEx779[T19D7, Pmyo-2::gfp]*
EG4248 *rund-1(ox281) X oxIs12[Punc-47:GFP, lin-15+] X*
EG4322 *ttTi5605 II ; unc-119(ed9) III*
EG4358 *cccp-1(ox334) III ; oxEx1113[RPCI94_09N13, Pmyo-2::gfp, lin-15(+)]*
EG4532 *egl-30(tg26) I*
EG4780 *cccp-1(e1122) III*
EG4781 *egl-30(tg26) I ; cccp-1(e1122) III*
EG4815 *gsa-1(ce81) I ; rund-1(ox281) X*
EG4816 *gsa-1(ce81) I ; rund-1(ox328) X*
EG4923 *lin-15(n765ts) X ; oxEx1134[Prund-1::GFP, lin-15(+)]*
EG4937 *rab-2(n501) I ; rund-1(ox281) X*
EG4938 *rab-2(n777) I ; rund-1(ox281) X*
EG4939 *egl-30(tg26) I rab-2(n501) I*
EG4940 *egl-30(tg26) I rab-2(n777) I*
EG4941 *rab-2(n501) I*
EG5003 *unc-119(ed9) III ; cxTi10882 IV*
EG5039 *rab-2(n3263) I ; rund-1(ox281) X*
EG5102 *egl-4(ks62) IV ; rund-1(ox281) X*
EG5103 *egl-4(ks62) IV ; rund-1(ox328) X*
EG5108 *ceh-17(np1) I ; rund-1(ox281) X*
EG5109 *ceh-17(np1) I ; rund-1(ox328) X*
EG5111 *rab-2(n3263) I ; rund-1(ox328) X*
EG5112 *rab-2(n3263) I ; egl-4(ks62) IV*
EG5170 *egl-4(ks62) IV*
EG5228 *nuIs183[Punc-129::NLP-21-Venus, Pmyo-2::GFP] III ; rund-1(ox281) X*
EG5231 *nuIs183[Punc-129::NLP-21-Venus, Pmyo-2::GFP] III ; rund-1(ox328) X*
EG5232 *rab-2(n3263) I ; nuIs183[Punc-129::NLP-21-Venus, Pmyo-2::GFP] III*
EG5258 *nuIs183[Punc-129::NLP-21-Venus, Pmyo-2::GFP] III cccp-1(ox334) III*
EG5260 *ceIs61[Punc-129::flp-3::venus, Punc-129::mCherry-snb-1, Pttx-3::mCherry] II ; rund-1(ox281) X*
EG5261 *ceIs61[Punc-129::flp-3::venus, Punc-129::mCherry-snb-1, Pttx-3::mCherry] II ; rund-1(ox328) X*
EG5334 *ceIs61[Punc-129::flp-3::venus, Punc-129::mCherry-snb-1, Pttx-3::mCherry] II ; cccp-1(ox334) III*
EG5340 *rab-2(nu415) I ; rund-1(ox281) X*
EG5341 *rab-2(nu415) I ; rund-1(ox328) X*
EG5348 *cccp-1(ox334) III ; rund-1(ox281) X*

EG5349 *cccp-1(ox334) III ; rund-1(ox328) X*
EG5505 *rund-1(tm3622) X*
EG5606 *oxIs590[Cb unc-119(+), Prund-1::rund-1(+)::tagRFP] II ; unc-119(ed9) III*
EG5608 *oxIs592[Cb unc-119(+), Prund-1::rund-1(+)::eGFP] II ; unc-119(ed9) III*
EG5609 *egl-30(tg26) I ; rund-1(tm3622) X*
EG5610 *egl-30(tg26) I rab-2(nu415) I*
EG5627 *rab-2(nu415) I*
EG5631 *oxIs590[Cb unc-119(+), Prund-1::rund-1(+)::tagRFP] II ; rund-1(tm3622) X*
EG5633 *oxIs592[Cb unc-119(+), Prund-1::rund-1(+)::eGFP] II ; rund-1(tm3622) X*
EG5635 *ceIs61[Punc-129::flp-3::venus, Punc-129::mCherry-snb-1, Pttx-3::mCherry] II ; rund-1(tm3622) X*
EG5636 *ceIs61[Punc-129::flp-3::venus, Punc-129::mCherry-snb-1, Pttx-3::mCherry] II ; egl-3(ok979) V ; rund-1(tm3622) X*
EG5644 *cccp-1(ox334) III ; egl-3(ok979) V*
EG5645 *egl-3(ok979) V ; rund-1(tm3622) X*
EG5647 *rab-2(nu415) I ; egl-3(ok979) V*
EG5648 *rab-2(nu415) I ; rund-1(tm3622) X*
EG5649 *rab-2(nu415) I ; cccp-1(ox334) III*
EG5674 *nuIs183[Punc-129::NLP-21-Venus, Pmyo-2::GFP] III ; rund-1(tm3622) X*
EG5745 *unc-119(ed9) III ; oxSi13[Prund-1::aman-2::eGFP, Cbunc-119] IV*
EG5748 *unc-119(ed9) III ; oxSi59[Prund-1::eGFP::tram-1, Cbunc-119] IV*
EG5805 *oxSi95[Prund-1::rund-1(+)::tdEos, Cb-unc-119] II ; unc-119(ed9) III*
EG5849 *oxSi95[Prund-1::rund-1(+)::tdEos, Cb-unc-119] II ; rund-1(tm3622) X*
EG5857 *egl-30(tg26) I ; unc-50(e306) III*
EG5858 *egl-30(tg26) I unc-74(ox78) I*
EG5859 *oxIs590[Cb unc-119(+), Prund-1::rund-1(+)::tagRFP] II ; oxSi13[Prund-1::aman-2::eGFP, Cbunc-119] IV*
EG5860 *oxIs590[Cb unc-119(+), Prund-1::rund-1(+)::tagRFP] II ; oxSi59[Prund-1::eGFP::tram-1, Cbunc-119] IV*
EG5912 *cccp-1(ox334) III ; nuIs195[Punc-129::ins-22::venus, Pmyo-2::gfp]*
EG5913 *nuIs195[Punc-129::ins-22::venus, Pmyo-2::gfp] ; rund-1(tm3622) X*
EG5914 *cccp-1(ox334) III ; ceIs72[Punc-129::ida-1::GFP, Pttx-3::mCherry]*
EG5915 *ceIs72[Punc-129::ida-1::GFP, Pttx-3::mCherry] ; rund-1(tm3622) X*
EG5936 *rab-2(nu415) I ; ceIs72[Punc-129::ida-1::GFP, Pttx-3::mCherry]*
EG5938 *rab-2(nu415) I ; nuIs195[Punc-129::ins-22::venus, Pmyo-2::gfp]*
EG6010 *ric-19(pk690) I ; rund-1(tm3622) X*
EG6193 *unc-119(ed9) III ; oxSi266[Prund-1::eGFP::rab-5, Cb unc-119] IV*
EG6244 *nuIs183[Punc-129::NLP-21-Venus, Pmyo-2::GFP] III ; egl-3(ok979) V ; rund-1(tm3622) X*
EG6286 *rab-2(nu415) I ; nuIs183[Punc-129::NLP-21-Venus, Pmyo-2::GFP] III ; rund-1(tm3622) X*
EG6359 *unc-119(ed9) III ; oxSi308[Prund-1::eGFP::rab-6.2, Cb-unc-119] IV*
EG6361 *unc-119(ed9) III ; oxSi310[Prund-1::eGFP::rab-7, Cb-unc-119] IV*
EG6362 *unc-119(ed9) III ; oxSi311[Prund-1::eGFP::rab-11.1, Cb-unc-119] IV*
EG6363 *unc-119(ed9) III ; oxSi312[Prund-1::eGFP::e-COP, Cb-unc-119] IV*
EG6364 *unc-119(ed9) III ; oxSi313[Prund-1::eGFP::syn-13, Cb-unc-119] IV*
EG6365 *unc-119(ed9) III ; oxSi314[Prab-2::eGFP::rab-2, Cb-unc-119] IV*
EG6366 *unc-119(ed9) III ; oxSi315[Prund-1::eGFP::syx-6, Cb-unc-119] IV*
EG6368 *rab-2(nu415) I ; oxSi314[Prab-2::eGFP::rab-2, Cb-unc-119] IV*
EG6369 *oxIs590[Cb unc-119(+), Prund-1::rund-1(+)::tagRFP] II ; oxSi266[Prund-1::eGFP::rab-5, Cb unc-119]* IV
EG6371 *oxIs590[Cb unc-119(+), Prund-1::rund-1(+)::tagRFP] II ; oxSi308[Prund-1::eGFP::rab-6.2, Cb-unc-119] IV*
EG6373 *oxIs590[Cb unc-119(+), Prund-1::rund-1(+)::tagRFP] II ; oxSi310[Prund-1::eGFP::rab-7, Cb-unc-119]* IV
EG6374 *oxIs590[Cb unc-119(+), Prund-1::rund-1(+)::tagRFP] II ; oxSi311[Prund-1::eGFP::rab-11.1, Cb-unc-119] IV*

EG6375 *oxIs590[Cb unc-119(+), Prund-1::rund-1(+)::tagRFP] II ; oxSi312[Prund-1::eGFP::e-COP, Cb-unc*-119] IV
EG6376 *oxIs590[Cb unc-119(+), Prund-1::rund-1(+)::tagRFP] II ; oxSi313[Prund-1::eGFP::syn-13, Cb-unc-119]* IV
EG6377 *oxIs590[Cb unc-119(+), Prund-1::rund-1(+)::tagRFP] II ; oxSi314[Prab-2::eGFP::rab-2, Cb-unc-119] IV*
EG6378 *oxIs590[Cb unc-119(+), Prund-1::rund-1(+)::tagRFP] II ; oxSi315[Prund-1::eGFP::syx-6, Cb-unc-119] IV*
EG6383 *oxSi314[Prab-2::eGFP::rab-2, Cb-unc-119] IV ; rund-1(ox281) X*
EG6384 *oxSi314[Prab-2::eGFP::rab-2, Cb-unc-119] IV ; rund-1(tm3622) X*
EG6388 *nuIs183[Punc-129::NLP-21-Venus, Pmyo-2::GFP] III ; rund-1(tm3622) X ; oxEx1520[Punc-129::rund-1::tagRFP, Pmyo-2::mCherry]*
EG6389 *rund-1(tm3622) X ; oxEx1521[Prund-1::RUNDC1 cDNA::tagRFP, Pmyo-2::gfp]*
EG6390 *rund-1(ox281) X ; oxEx1522[Prund-1::RUNDC1 cDNA::tagRFP, Pmyo-2::gfp]*
EG6391 *rund-1(tm3622) X ; oxEx1523[Phsp16.2::rund-1 cDNA::tagRFP, Pmyo-2::gfp]*
EG6652 *rund-1(tm3622) X ; oxEx1575[Prund-1::rund-1(+)::tdEos, Pmyo-2::gfp]*
EG6917 *oxIs590[Cb unc-119(+), Prund-1::rund-1(+)::tagRFP] II ; cccp-1(ox334) III*
EG6920 *cccp-1(ox334) III ; oxSi314[Prab-2::eGFP::rab-2, Cb-unc-119] IV*
EG6922 *oxSi315[Prund-1::eGFP::syx-6, Cb-unc-119] IV ; rund-1(tm3622) X*
EG6923 *oxSi308[Prund-1::eGFP::rab-6.2, Cb-unc-119] IV ; rund-1(tm3622) X*
EG6927 *rab-2(nu415) I ; oxIs590[Cb unc-119(+), Prund-1::rund-1(+)::tagRFP] II*
EG6929 *oxSi503[Prund-1::rund-1 CC::tagRFP, Cb-unc-119] II ; unc-119(ed9) III*
EG6933 *rund-1(tm3622) X ; oxEx1366[Cb-unc-119(+) cccp-1::eGFP, Pmyo-2::mCherry, Pmyo-3::mCherry, Prab-3::mCherry]*
EG6934 *rab-2(nu415) I ; oxEx1366[Cb-unc-119(+) cccp-1::eGFP, Pmyo-2::mCherry, Pmyo-3::mCherry, Prab-3::mCherry]*
EG6941 *oxSi503[Prund-1::rund-1 CC::tagRFP, Cb-unc-119] II ; rund-1(tm3622) X*
EG6943 *oxSi505[Prund-1::rund-1 RUN::tagRFP, Cb-unc-119] II ; unc-119(ed9) III*
EG6945 *oxSi505[Prund-1::rund-1 RUN::tagRFP, Cb-unc-119] II ; rund-1(tm3622) X*
EG6949 *cccp-1(ox334) III ; oxEx1622[Prab-3::cccp-1::gfp, Prund-1::rund-1::tagRFP]*
EG6951 *cccp-1(ox334) III ; oxEx1624[Prab-3::cccp-1::gfp, Prab-3::tagRFP::rab-2(DA)]*
EG6953 *cccp-1(ox334) III ; oxEx1626[Prab-3::cccp-1::gfp, Prab-3::tagRFP::rab-2(DN)]*
EG6982 *cccp-1(ox334) III ; oxEx1628[Prab-3::cccp-1::gfp, Punc-122::gfp]*
EG7187 *unc-119(ed9) III ; oxEx1366[Cb-unc-119(+) cccp-1::eGFP, Pmyo-2::mCherry, Pmyo-3::mCherry, Prab-3::mCherry]*
EG7227 *lin-15(n765ts) X ; oxEx1251[Pcccp-1::gfp, lin-15(+)]*
EG7242 *rund-1(ox281) X lin-15(n765ts) X ; oxEx1197[Prab-3::rund-1 cDNA::mCherry, lin-15(+)]*
EG7244 *rund-1(ox281) X lin-15(n765ts) X ; oxEx1260[Pvha-6::rund-1 cDNA::mCherry, lin-15(+)]*
EG7249 *eri-1(mg366) IV ; lin-15(n744) X*
FK234 *egl-4(ks62) IV*
IB16 *ceh-17(np1) I*
GQ640 *ric-19(ok833) I ; nuIs183[Punc-129::NLP-21-Venus, Pmyo-2::GFP] III*
GQ641 *tbc-8(tm3802) III nuIs183[Punc-129::NLP-21-Venus, Pmyo-2::GFP] III*
GQ693 *nuIs183[Punc-129::NLP-21-Venus, Pmyo-2::GFP] III ; rund-1(tm3622) X*
GQ698 *ric-19(ok833) I ; nuIs183[Punc-129::NLP-21-Venus, Pmyo-2::GFP] III ; rund-1(tm3622) X*
GQ699 *tbc-8(tm3802) III nuIs183[Punc-129::NLP-21-Venus, Pmyo-2::GFP] III ; rund-1(tm3622) X*
KG421 *gsa-1(ce81) I*
KG1395 *nuIs183[Punc-129::NLP-21-Venus, Pmyo-2::GFP] III*
KG1475 *rab-2(ce365) I ; nuIs183[Punc-129::NLP-21-Venus, Pmyo-2::GFP] III*
KG1624 *nuIs195[Punc-129::ins-22::venus, Pmyo-2::gfp]*
KG1645 *ceIs61[Punc-129::flp-3::venus, Punc-129::mCherry-snb-1, Pttx-3::mCherry] II*
KG1655 *rab-2(ce365) I ; ceIs61[Punc-129::flp-3::venus, Punc-129::mCherry-snb-1, Pttx-3::mCherry] II*
KG1852 *ceIs72[Punc-129::ida-1::GFP, Pttx-3::mCherry]*
MT1093 *rab-2(n501) I*
MT1656 *rab-2(n777) I*
N2 Bristol wild-isolate, standard lab wild type

NL2003 *ric-19(pk690) I*
VC671 *egl-3(ok979) V*
XZ1022 *rab-2(nu415) I; oxIs590[Cb unc-119(+), Prund-1::rund-1(+)::tagRFP] II ; oxSi266[Prund-1::eGFP::rab-5, Cb unc-119]* IV
XZ1023 *rab-2(nu415) I; oxIs590[Cb unc-119(+), Prund-1::rund-1(+)::tagRFP] II ; oxSi308[Prund-1::eGFP::rab-6.2, Cb-unc-119] IV*
XZ1024 *rab-2(nu415) I; oxIs590[Cb unc-119(+), Prund-1::rund-1(+)::tagRFP] II ; oxSi310[Prund-1::eGFP::rab-7, Cb-unc-119]* IV
XZ1026 *rab-2(nu415) I; nuIs183[Punc-129::NLP-21-Venus, Pmyo-2::GFP] III*
XZ1027 *nuIs183[Punc-129::NLP-21-Venus, Pmyo-2::GFP] III cccp-1(ox334) III; rund-1(tm3622)*
XZ1028 *rab-2(nu415); nuIs183[Punc-129::NLP-21-Venus, Pmyo-2::GFP] III cccp-1(ox334) III*
ZH382 *rab-2(n3263) I*

List of plasmids

Miscellaneous plasmids

RPCI94_09N13	BAC carrying the *C. briggsae* ortholog of *cccp-1*, used to make *oxEx1113* (10 ng/μl)
T19D7	cosmid carrying the *rund-1* gene T19D7.4, used to make *oxEx779* (10 ng/μl)
yk471g7	*rund-1* full length cDNA
yk530g8	*cccp-1b* full length cDNA
Prab-3::tagRFP::rab-2(DA) used to make oxEx1624 (5 ng/μl)	
Prab-3::tagRFP::rab-2(DN) used to make oxEx1626 (5 ng/μl)	

Gateway destination vectors

pCFJ150	Gateway destination vector for insertion at chromosome II Mos site *ttTi5605*
pCFJ201	Gateway destination vector for insertion at chromosome IV Mos site *cxTi10882*
pDEST-R4-R3	Gateway destination vector

Gateway entry clones

pCM1.56	*Phsp-16.2* [4-1] (493 bp of the *hsp-16.2* promoter upstream of the ATG)
pCR110	*GFP* [1-2]
pENTR[4-1] P[rab-3]	*Prab-3* [4-1] (1224 bp of the *rab-3* promoter upstream of and including the ATG)
pGH107	*tagRFP::let-858* 3'UTR [2-3]
pGH112	*eGFP::let-858* 3'UTR [2-3]
pGH115	*eGFP* [1-2]
pGH271	*tdEos::let-858* 3'UTR [2-3]
pMA15	*Pcccp-1* [4-1] (1696 bp of the *cccp-1* promoter upstream of and including the ATG)
pMA18	*cccp-1b* cDNA [1-2] (from yk530g8)
pMA20	*rund-1* cDNA [1-2] (from yk471g7)
pMA108	*rab-5* cDNA::let-858 3'UTR [2-3]
pMA115	*rab-7* cDNA::let-858 3'UTR [2-3]
pMA116	*rab-11.1* cDNA::let-858 3'UTR [2-3]
pMA132	*rab-6.2* cDNA::let-858 3'UTR [2-3]
pMA145	*syx-6* cDNA::let-858 3'UTR [2-3]
pMA157	RUNDC1 cDNA[1-2]
pMA165	*rund-1* coiled-coil domain [1-2] (aa 1-261)
pMA166	*rund-1* RUN domain [1-2] (aa 262-549)
pPM1	*aman-2* [1-2]
pPM2	*tram-1* [2-3]
pSD11	*Prab-2* [4-1] (3237 bp of the *rab-2* promoter upstream of the ATG)
pSD12	*Punc-129* [4-1] (2645 bp of the *unc-129* promoter upstream of the ATG)
pSD16	*rab-2*(+) gene with introns and *rab-2* 3'UTR [2-3]
pSD25	*syn-13* with *let-858* 3'UTR [2-3]
pSD26	ε-COP with let-858 3'UTR [2-3]
pT19D7.4 [4-1]	*Prund-1* [4-1] (2733 bp of the *rund-1* promoter upstream of and including the ATG)

pT19D7.4 [1-2] *rund-1(+)* gene with introns [1-2]
p_VW02B12L.1_93 *Pvha-6* [4-1] (881 bp of the *vha-6* promoter upstream of and including the ATG)

Gateway expression constructs

pAP4	*Prund-1::gfp*	used to make *oxEx1134* (10 ng/μl)
pMA17	*Pcccp-1::gfp*	used to make *oxEx1251* (10 ng/μl)
pMA24	*Prab-3::rund-1* cDNA::mCherry	used to make *oxEx1197* (10 ng/μl)
pMA38	*Pvha-6::rund-1* cDNA::mCherry	used to make *oxEx1260* (10 ng/μl)
pMA56	*Prund-1::rund-1(+)::tagRFP*	used to make *oxIs590* and *oxEx1622* (10 ng/μl)
pMA57	*Prund-1::rund-1(+)::eGFP*	used to make *oxIs592*
pMA58	*Pcccp-1::cccp-1 cDNA::eGFP*	used to make *oxEx1366* (50 ng/ml)
pMA74	*Prund-1::aman-2::eGFP*	used to make *oxSi13*
pMA75	*Prund-1::eGFP::tram-1*	used to make *oxSi59*
pMA90	*Prund-1::rund-1(+)::tdEos*	used to make *oxEx1575* (10 ng/μl) & *oxSi95*
pMA112	*Prund-1::eGFP::rab-5*	used to make *oxSi266*
pMA118	*Prund-1::eGFP::rab-7*	used to make *oxSi310*
pMA119	*Prund-1::eGFP::rab-11.1*	used to make *oxSi311*
pMA138	*Prund-1::eGFP::rab-6.2*	used to make *oxSi308*
pMA147	*Prund-1::eGFP::syx-6*	used to make *oxSi315*
pMA150	*Phsp16.2::rund-1 cDNA::tagRFP*	used to make *oxEx1523* (10 ng/μl)
pMA152	*Punc-129::rund-1 cDNA::tagRFP*	used to make *oxEx1520* (10 ng/μl)
pMA159	*Prab-3::cccp-1 cDNA::eGFP*	used to make *oxEx1622, oxEx1624, oxEx1626, oxEx1628* (10 ng/μl)
pMA161	*Prund-1::RUNDC1 cDNA::tagRFP*	used to make *oxEx1521 & oxEx1522* (10 ng/μl)
pMA172	*Prund-1::rund-1 CC::tag RFP*	used to make *oxSi503*
pMA173	*Prund-1::rund-1 RUN::tagRFP*	used to make *oxSi505*
pSD18	*Prab-2::eGFP::rab-2(+)*	used to make *oxSi314*
pSD30	*Prund-1::eGFP::syn-13*	used to make *oxSi313*
pSD31	*Prund-1::eGFP::ε-COP*	used to make *oxSi312*

Supplemental References

Edgar, R.C. (2004). MUSCLE: multiple sequence alignment with high accuracy and high throughput. Nucleic Acids Res *32*, 1792–1797.

Frøkjaer-Jensen, C., Davis, M.W., Hopkins, C.E., Newman, B.J., Thummel, J.M., Olesen, S.-P., Grunnet, M., and Jorgensen, E.M. (2008). Single-copy insertion of transgenes in Caenorhabditis elegans. Nat. Genet *40*, 1375–1383.

Liu, Q., Hollopeter, G., and Jorgensen, E.M. (2009). Graded synaptic transmission at the Caenorhabditis elegans neuromuscular junction. Proc. Natl. Acad. Sci. U.S.A. *106*, 10823–10828.

Mello, C.C., Kramer, J.M., Stinchcomb, D., and Ambros, V. (1991). Efficient gene transfer in C.elegans: extrachromosomal maintenance and integration of transforming sequences. EMBO J *10*, 3959–3970.

Rostaing, P., Weimer, R.M., Jorgensen, E.M., Triller, A., and Bessereau, J.-L. (2004). Preservation of immunoreactivity and fine structure of adult C. elegans tissues using high-pressure freezing. J. Histochem. Cytochem *52*, 1–12.

Watanabe, S., Punge, A., Hollopeter, G., Willig, K.I., Hobson, R.J., Davis, M.W., Hell, S.W., and Jorgensen, E.M. (2011). Protein localization in electron micrographs using fluorescence nanoscopy. Nat. Methods *8*, 80–84.